

1 This manuscript has been submitted for publication in GEOMORPHOLOGY. Please note that, despite having undergone peer-
2 review, the manuscript has yet to be formally accepted for publication. Subsequent versions of this manuscript may have slightly
3 different content. If accepted, the final version of this manuscript will be available via the 'Peer-reviewed Publication DOI' link on the
4 right-hand side of this webpage. Please feel free to contact any of the authors; we welcome feedback.

5

6

7

8 **Modeling the spatial dynamics of marsh ponds in New England salt marshes**

9

10 G. Mariotti^{1,2}, A.C. Spivak³, S.Y. Luk⁴, G. Ceccherini⁵, M. Tyrrell⁶, M. Eagle Gonneea⁷

11

12 1. Louisiana State University, Department of Oceanography and Coastal Sciences, Baton Rouge (LA),

13

USA

14 2. Louisiana State University, Center for Computation and Technology, Baton Rouge (LA), USA

15

3. University of Georgia, Department of Marine Sciences, Athens (GA), USA

16 4. Woods Hole Oceanographic Institution, Department of Marine Chemistry and Geochemistry, Woods

17

Hole (MA), USA

18

5. Joint Research Centre, Bioeconomy Unit, European Commission, Ispra, Italy

19

6. Waquoit Bay National Estuarine Research Reserve, Falmouth (MA), USA

20

7. U.S. Geological Survey, Woods Hole (MA), USA

21

22

Corresponding author: Giulio Mariotti, gmariotti@lsu.edu

23

Abstract

24 Ponds are common features on salt marshes, yet it is unclear how they affect large-scale marsh evolution.

25 We developed a spatially explicit model that combines cellular automata for pond formation, expansion,

26 and drainage, and partial differential equations for elevation dynamics. We use the mesotidal Barnstable

27 marsh (MA, USA) as a case study, for which we measured pond expansion rate by remote sensing

28 analysis over a 41-year time span. We estimated pond formation rate by comparing observed and modeled

29 pond size distribution, and predicted pond deepening by comparing modeled and measured pond depth.

30 The Barnstable marsh is currently in the pond recovery regime, i.e., every pond revegetates and recovers

31 the necessary elevation to support plant growth after re-connecting to the channel network. This pond
32 dynamic creates an equivalent (i.e., spatially and temporally averaged over the whole marsh) 0.5-2 mm/yr
33 elevation loss that needs to be supplemented by excess vertical accretion. We explore how the pond
34 regime would change with decreased sediment supply and increased relative sea-level rise (RSLR) rate,
35 focusing on the case in which the vegetated marsh keeps pace with RSLR. When the RSLR rate remains
36 below the minimum unvegetated deposition rate, the pond dynamics is nearly unaltered and ponds always
37 occupy ~10% of the marsh area. However, when RSLR rate exceeds this threshold, the ponds in the
38 marsh interior – which receive the least amount of suspended sediment – do not recover after drainage.
39 These ponds transition to mudflats and permanently occupy up to 30% of the marsh area depending on
40 RSLR rate. For marshes with a small tidal range, such as the microtidal Sage Lot Pond marsh on the
41 opposite side of the peninsula from Barnstable marsh, high RSLR rates could bring every portion of the
42 marsh into the pond runaway regime, with the whole marsh eventually converting into mudflats. In this
43 regime, the existing marsh would disappear within centuries to millennia depending on the RSLR rate.
44 Because of the spatial and temporal components of marsh evolution, a single RSLR threshold value
45 applied across the entire marsh landscape provides a limited description of the marsh vulnerability to

46 RSLR.

47

48

49

50

51 **1. Introduction**

52 Marsh evolution models commonly assume a homogenous marsh platform, in which both elevation and
53 plant biomass change smoothly except close to a few ecotones (Marani et al., 2013). On the contrary,
54 many marsh platforms are highly heterogeneous because of the presence of ponds – semicircular
55 depressions permanently inundated even at low tide. This heterogeneity is particularly relevant for the
56 Mid-Atlantic and New England coast of the USA, where ponds are ubiquitous features (Adamowicz and
57 Roman, 2005; Harshberger, 1909; Koop-Jakobsen and Gutbrod, 2019; Redfield, 1972; Schepers et al.,
58 2017). Thus, considering the presence of ponds is necessary to accurately predict the landscape-level
59 evolution and persistence of these salt marshes under climate change.

60 Ponds haven been simulated in a simplified 2D model (Kirwan et al., 2008) by lowering the elevation and
61 preventing vegetation growth in a few random locations on the marsh platform. After this temporary
62 disturbance, the vegetation was allowed to regrow and the bed quickly regained its original elevation by
63 accreting faster than RSLR rate. Because of these localized and temporary bursts of vertical accretion, the
64 model provided a simple explanation for the presence of spatial heterogeneities in marsh vertical
65 accretion and for the widely observed mismatch between marsh vertical accretion and RSLR.
66 Nonetheless, the model overlooked several physically-based processes that play a key role in pond
67 dynamics: pond deepening by organic matter oxidation, pond expansion by erosion of the pond edge, and
68 pond drainage by channel interception.

69 A simple lumped model that considered the evolution of a single pond (Mariotti, 2016) suggested that
70 marshes are either in a regime of pond recovery where ponds form, expand, reconnect with the nearby
71 tidal creek and recover to the surrounding marsh elevation, or in a regime of pond runaway (also called
72 pond collapse regime) in which ponds do not revegetate and marsh area is lost even if the vegetated
73 platform keeps pace with sea-level rise. Vertical accretion by *in situ* plant production does not contribute
74 to pond recovery if, at the time of pond drainage, the elevation of the pond bed is below the limit for
75 vegetation growth, which is roughly equal to mean sea level along the Atlantic and Gulf Coast of the

76 USA (McKee and Patrick, 1988). Indeed, if the bed elevation lies below the limit for vegetation growth,
77 vertical accretion is only provided by deposition of suspended sediment. Vertical accretion by *in situ* plant
78 production would be present only after the elevation deficit for vegetation growth is overcome.
79 Accordingly, the model found that the marsh enters the pond runaway regime when the RSLR rate is
80 larger than the minimum unvegetated accretion rate (Mariotti, 2016), which is equal to $C \cdot r / (2T \cdot \rho_m)$, where
81 C is the suspended sediment concentration, r is the tidal range, T is the tidal period, and ρ_m is the mud dry
82 bulk density. Marshes are thus more likely to be in the pond runaway regime if the tidal range is small,
83 but a very large sediment supply can allow for pond recovery in microtidal systems, as shown by an
84 example in coastal Louisiana (Mariotti, 2016). A major limitation of the model, however, was that it
85 neglected the interactions between multiple ponds, which likely represent important spatial dynamics over
86 long time scales. As a consequence, the model was not able to predict spatially averaged metrics, such as
87 the amount of pond area on the marsh platform in the pond recovery regime or the rate of pond area
88 increase in the pond runaway regime.

89 When considering the dynamics of ponds, it is also important to simulate key aspects of sediment
90 transport. For example, it is crucial to simulate how the suspended sediment concentration (SSC) that
91 drives inorganic deposition (i.e., mud) varies in space, such as the SSC decreases with distance from the
92 channels (Christiansen et al., 2000; Fagherazzi et al., 2012), thus making the marsh interior more
93 susceptible to entering the pond runaway regime. In addition, lateral sediment redistribution by soil
94 diffusion (or soil creep), which is present along marsh boundaries with sharp elevation gradients such as
95 the banks tidal creeks (Kirwan and Murray, 2007; Mariotti, 2018; Mariotti et al., 2019, 2016), could
96 transfer sediment from high to low elevation areas and thus affect the rate of vertical elevation change.

97 Another important aspect to consider is the biogeochemical dynamics of ponds. The emergent vegetation
98 that dominates the marsh platform (e.g., *Spartina alterniflora*, *S. patens*, *Distichlis spicata*, etc.) cannot
99 survive in ponds because of inundation stress or because of the high salinity that results from the absence
100 of regular flushing (Pethick, 1974). Instead, ponds in New England marshes are colonized by

101 communities of micro- and macro-algae and submerged grasses such as *Ruppia maritima* (Harshberger,
102 1909; Spivak et al., 2017). The organic matter composition of pond surface sediments reflects inputs from
103 algal and plant communities that colonize ponds during formation (Spivak et al., 2018). Yet, the
104 contribution of submerged algae and grasses to vertical accretion in ponds is likely negligible, given that
105 ponds tend to be net heterotrophic (Spivak et al., 2017) and thus do not accumulate carbon but rather
106 remove the existing one.

107 In addition to the absence of vertical accretion, ponds might actually experience a net elevation loss.
108 Indeed, the high rates of respiration, driven primarily by sulfate reduction (van Huissteden and van de
109 Plassche 1998), convert buried organic matter into dissolved inorganic carbon and thereby contribute to
110 soil column collapse and pond deepening (Johnston et al., 2003; Spivak et al., 2018, 2017). The elevation
111 trajectory of ponds is thus diametrically opposite to that of the marsh platform, which gains elevation
112 through time via suspended sediment deposition and *in situ* plant production. As a result, ponds in New
113 England marshes are likely experiencing a gradual deepening with respect to the surrounding marsh
114 platform (Wilson et al., 2009, 2010).

115 Here, we develop a spatially explicit model for pond dynamics. We apply the model to the Barnstable
116 marsh (MA, USA), which is a typical mesotidal marsh in New England, and constrain the model with
117 field data and remote sensing analysis. We also consider the case with a smaller tidal range, using as
118 reference a nearby microtidal marsh with limited sediment supply (the Sage Lot Pond marsh). Then, we
119 explore the model for different RSLR rates and sediment supply to predict future marsh trajectories. As
120 suggested by a previous idealized model (Mariotti, 2016), we expect to find a threshold above which
121 ponds never revegetate and thus lead to permanent marsh loss. By including pond dynamics within the
122 model, we predict marsh loss when the marsh complex enters the runaway pond regime, which occurs
123 even when deposition on the vegetated marsh platform is equal or greater than the RSLR rate, a
124 commonly used threshold for marsh drowning (Morris et al., 2002).

125 **2. Site description**

126 The study area is in the New England region of the United States, which experiences a temperate climate,
127 about 1000 mm of precipitation per year, a growing season from May to September, and overnight freezes
128 during the winter (Mariotti et al., 2019). Ice rafting has been documented to occur, especially in
129 concomitance with winter storm surges (Argow et al., 2011).

130 Barnstable is a mesotidal backbarrier marsh, located on the north side of the Cape Cod peninsula (Fig. 1).
131 The spring tidal range is about 3.6 m (NOAA Sesuit Harbor station 8447241). The marsh is dominated by
132 *S. alterniflora* in the low marsh and *S. patens* in the high marsh (Redfield, 1972). The majority of the
133 Barnstable marsh has been ditched since the early 1900s. For simplicity, in this study we focus on an area
134 that does not have man-made ditches (Fig. 1). This choice allows us to isolate and understand the spatially
135 explicit pond dynamics under natural conditions, without the confounding effects of mechanical
136 anthropogenic disturbances.

137 Sage Lot Pond is a polyhaline, microtidal (0.7 m spring tidal range, NOAA Woods Hole Station 8447930)
138 backbarrier marsh located on the south side of the Cape Cod peninsula (Fig. 1). The marsh is dominated
139 by short form *S. alterniflora* on the low marsh and *Distichilis spicata*, *Juncus gerardii*, and some *S.*
140 *patens* at higher elevations (Gonneea et al. 2019). This marsh is also ditched.

141 According to the nearby NOAA station 8443970, mean sea level was -9.2 cm in the NAVD88 datum
142 during the epoch 1983-2001. Considering the recent increase in sea level, we assume that MSL is now at
143 0 m NAVD88, which agrees with the datum analysis in the nearby Plum Island Estuary marsh
144 (Hopkinson et al., 2018).

145 **3. Methods**

146 **3.1 Field measurements and remote sensing analysis**

147 For the Barnstable marsh, suspended sediments in tidal creek water were collected in triplicate 1-liter pre-
148 combusted (450 °C) glass bottles from four different locations (Fig. 1) between June 21st and August 1st
149 2018. All samples were collected during the incoming tide. Samples were filtered through pre-combusted
150 and pre-weighed glass fiber filters (nominal pore size 0.45 µm). The filters were then dried to constant

151 mass (60 °C) and concentrations were calculated by normalizing suspended sediment mass to the volume
152 filtered. While this sampling is not a comprehensive characterization of the sediment dynamics, it
153 provides at least a magnitude estimate, which is often the only data available (Cavatorta et al., 2003).

154 Sediment cores were collected from three transects at approximately 2 m (channel adjacent) and 100 m
155 (marsh interior) from the creek bank (Table 1). All cores were taken in the vegetated platform, i.e., not in
156 a pond. Cores were collected with a modified piston core where a plastic core liner (11 cm diameter) was
157 fitted with a gasketed piston and placed on the sediment surface. The core liner was pushed ~70 cm into
158 the marsh subsurface while the piston was maintained at the surface to minimize compaction, which was
159 observed through the clear core liner. The cores were split vertically, sampled at 1 cm intervals to 45 cm
160 below soil surface and 2 cm intervals thereafter, frozen, and then freeze-dried. Sediment samples were
161 prepared for gamma analysis by sealing approximately 5 g of dried, homogenized peat for 3 weeks, and
162 counting on a planar-type gamma counter for 24 to 48 hours to measure ^7Be , ^{137}Cs , ^{210}Pb , and ^{226}Ra at
163 477, 661.6, 46.5 and 352 KeV energies respectively (Canberra Inc., USA). Detector efficiency was
164 determined from EPA standard pitchblende ore in the same geometry as the samples. Activities of ^7Be ,
165 ^{137}Cs , and ^{210}Pb were decay corrected to time of collection. Suppression of low energy peaks by self-
166 adsorption was corrected for according to (Cutshall et al., 1983). Excess ^{210}Pb was calculated by
167 subtracting supported ^{226}Ra from total ^{210}Pb with a detection limit of 0.1 dpm g⁻¹. Sediment ages were
168 calculated using the continuous rate of supply ^{210}Pb age model, a variant on the advection-decay equation
169 (Appleby and Oldfield, 1978). This age model assumes that ^{210}Pb down-core activity is a function of
170 decay and variable sediment accretion, however, the full ^{210}Pb profile must be captured to prevent bias
171 towards ages that are too old and accretion rates that are too low at depth (Binford, 1990). Vertical
172 accretion rates were calculated as the age difference between each interval, with temporal resolution
173 typically 2 to 10 years depending on marsh, treatment, and sediment age.

174 Ponds within a few hundred meters from the sites where cores were collected were surveyed in the
175 summer of 2019 in one of two ways (Fig. 1G). First, 200 marsh-pond boundaries were surveyed in 2019

176 by measuring the elevation of the marsh adjacent to the pond edge and the elevation of the pond bed
177 adjacent to the pond edge using an RTK-GPS with vertical accuracy of 2 cm. The height of the pond bank
178 was calculated as the difference between these measurements. Second, elevation transects running
179 through the diameter of the pond were surveyed for thirteen of the 200 ponds (five small, five medium,
180 and three large ponds). The absolute bed elevation was referenced to the elevation of the adjacent marsh
181 surface, which was surveyed with the RTK-GPS.

182 We performed a remote sensing analysis using two datasets: USGS Single Frames Aerial Photos from
183 March 1973 with resolution of ~0.5 m and USGS high resolution orthoimages from April 2014 with
184 resolution of 0.075 m, both of which were collected at low tide (earthexplorer.gov). We also used USGS
185 Lidar collected in 2014 with resolution of 1 m (OCM Partners, 2019). For consistency we resampled all
186 datasets to a 1 m resolution. In both images we defined isolated ponds as those cells with standing water
187 at low tide, which were easily identifiable using a threshold on the intensity of the visible band. Pond
188 cells were clustered together using a five-point stencil connection, such that pond cells that touched each
189 other either on the top, bottom, right, or left boundary were grouped together. Then, we identified the
190 same ponds in each image and calculated the rate of area change. We excluded from the analysis those
191 ponds that either merged together or reconnected to the channel network between 1973 and 2014. From
192 the rate of area change, we calculated the equivalent rate of pond radius expansion. Change was measured
193 as a difference in area rather than the retreat of the pond edge, eliminating any error due to image
194 misalignment.

195 For the Sage Lot Pond marsh, SSC was measured from 2011 to 2018 across all seasons and tides. A total
196 of 258 grab samples (500 mL each) were collected and stored at 4 °C for a maximum of 1 week and then
197 filtered through pre-combusted borosilicate glass fiber filters (0.7 um pore size), rinsed thoroughly with
198 deionized water to remove salts, and dried at 105 °C for >4h. SSC was determined as the ratio of dried
199 filtrate mass total per sample volume. Existing vertical accretion measurements for Sage Lot Pond marsh
200 (Gonneea et al., 2019, 2018) are also reported in Table 1.

201 3.2 Model for pond dynamics

202 Within the model, the pond dynamics is implemented as a cellular automata, in which each cell is
203 described by its state (which can only take a finite number of values) without explicitly simulating the
204 elevation. Channels are special cells that are fixed in time, which do not widen, narrow, or migrate
205 laterally. These cells don't take part in the evolution of the cellular automata and are collectively defined
206 as "channel network". Cells that are not part of the channel network are marsh cells, which collectively
207 constitute the marsh domain. Marsh cells are either connected or isolated. Connected cells experience
208 tidal fluctuations, and are defined as vegetated platform if their elevation is above the lower limit for
209 vegetation growth (z_{min}) or mudflat if their elevation is below (z_{min}). Isolated cells, also called isolated
210 ponds or ponds, do not experience tidal fluctuations or exchange with the channel network. Pond cells
211 with an elevation below z_{min} are defined as drowned ponds (Fig. 2).

212 Two processes allow for connected marsh cells to become isolated cells: pond formation and pond
213 expansion. In the real marsh, formation of new ponds can take place by a variety of mechanisms. A slight
214 depression in the marsh might lead to water logging and rapid decay of the marsh peat. Deposition of rafts
215 composed of either eroded plant material or macroalgae might kill the standing vegetation and
216 temporarily prevent new plant growth (Pethick, 1974). Ice rafting might compress the marsh (Argow and
217 FitzGerald, 2006) or remove large pieces of standing vegetation. Sub-surface piping might collapse the
218 marsh from below (Kesel and Smith, 1978). Large patches of vegetation can be removed by grazers such
219 a geese herbivory (Kirwan et al., 2008) and major storms (Howes et al., 2010). Rather than explicitly
220 modeling these different mechanisms, we simply assume that individual ponds form at a constant rate k_{seed}
221 [#ponds/m²/yr], that is, during each time step Δt , each vegetated marsh cell is transformed into a pond cell
222 with a probability $k_{seed}\Delta t\Delta x^2$. Pond expansion allows existing ponds (i.e., clusters of connected pond cells)
223 to enlarge. This process is implemented at every boundary between a pond cell and a vegetated cell.
224 Expansion is simulated using a probabilistic approach (Mariotti and Canestrelli, 2017), in which a

225 vegetated cell adjacent to a pond cell is converted to a pond cell with a probability $p=k_{exp}\Delta t/\Delta x$, where k_{exp}
226 is the expansion rate [m/yr].

227 Pond cells transform into vegetated cells though pond drainage. In the real marsh, pond drainage occurs
228 when a pond become close enough to the channel network that a new connecting channel forms, as
229 exemplified in Fig. 1E. Then, the pond fills in quickly (assuming that there is enough sediment supply)
230 and the connecting channel, now lacking the tidal prism associated with the pond, eventually silts in. The
231 model is unable to explicitly simulate the formation or closure of these transient connecting channels,
232 since the model does not simulate tidal hydrodynamics and the main channel network is assumed to be
233 fixed in time. We thus parameterize this effect by assuming that pond drainage instantaneously occurs
234 when a connected cell becomes closer than a critical distance L from the channel network. When this
235 happens, the whole pond, which consists of all pond cells that are contiguous to at least one pond cell
236 with distance L from the channel network, are drained and all its cells become connected cells. The
237 distance L is the distance at which the pressure gradient generated by the water in the pond is able to start
238 scouring the marsh soil – possibly by seepage and piping first – and eventually form a connecting
239 channel. In theory this distance might be calculated using a hydrodynamic and sediment transport model,
240 but for simplicity this distance is calibrated to reproduce the observation that ponds tend to drain when
241 they get about 20 m away from the main channel network (Fig. 1E).

242 **3.3 Model for elevation dynamics**

243 The elevation of each marsh cell relative to mean sea level, $z(x,y,t)$, is described as

$$244 \quad \frac{dz}{dt} = D_p + D_m - S - P - R \quad (\text{Eq. 1})$$

245 where D_p is the *in situ* organic accretion by marsh plants, D_m is the accretion from suspended sediment,
246 which we assume is composed of mud and thus transported in suspension, S is the divergence of the creep
247 flux F , P is the elevation loss by pond dynamics (which is further explained below), and R is the relative
248 sea-level rise rate.

249 The organic accretion by *in situ* plant production is $D_p = D_{pMAX}B$, where D_{pMAX} is the maximum accretion
 250 rate [mm/yr] and B is a function that describes the dependence on the bed elevation and serves as a proxy
 251 for the hydroperiod, $B = \max[0, 4(z - z_{min})(z_{max} - z)/(z_{max} - z_{min})^2]$, where z_{min} and z_{max} are the
 252 minimum and maximum elevation for vegetation growth. B is set equal to zero in isolated ponds,
 253 simulating the absence of marsh plants and assuming that any macrophytes and microphytobenthos
 254 present in ponds do not contribute to substantial vertical accretion.

255 Mud accretion depends on hydroperiod and the local SSC. The spatial pattern of SSC is described by

$$256 \quad C = C_o(\alpha + (1 - \alpha)e^{-\beta l}) \quad (\text{Eq. 2})$$

257 where C_o is the time-average suspended sediment concentration in the channels, $l(x,y)$ is the distance to
 258 the closest cells that belong to the channel network, β is the decay factor for SSC with distance from the
 259 channel network, and α is the factor describing the SSC that is spatially uniform. This last parameter
 260 allows transport of sediment even to large distances from the channels, and thus can parameterize
 261 processes such as storm-induced deposition on the marsh platform. Mud accretion thus equals

$$262 \quad D_m = \frac{C_{min}(h,r)\min(1, h/\Delta r)}{T\rho_m} \quad (\text{Eq. 3})$$

263 where h is the depth with respect to MHHW, T is the tidal period, ρ_m is the dry bulk density of the mud,
 264 and Δr is the difference between the spring and neap high tide. The last factor in the numerator is
 265 introduced to account for modulation introduced by the spring-neap variability. If the marsh elevation is
 266 at least Δr lower than MHHW, the marsh is inundated every tidal cycle and this factor is equal to one. If
 267 the marsh is higher than this elevation, the marsh is only inundated during spring tides, and the factor will
 268 be less than one. This allows mud to deposit at high marsh elevations but at a lower rate.

269 In theory, ponds could accrete vertically by suspended sediment deposition akin to the marsh platform.

270 Yet, several reasons suggest that this deposition is small. First, despite ponds having a large depth, the
 271 water in the pond is not exchanged during tides. Only the thin layer of water that flows over the pond

272 should count toward sediment deposition as formulated in Eq. 3 (which assumes that the water depth is
273 equal to the depth of the flow that floods that cell). Second, ponds lack the emergent marsh vegetation
274 that enhances sediment trapping. As a consequence, for the same water depth and sediment concentration,
275 a vegetated pond should experience a lower sediment deposition than a vegetated marsh. Third, ponds are
276 generally far from channels, specifically they are always farther than the distance L . As such, the
277 suspended sediment concentration above ponds is always lower than on the marsh close to the channel
278 edge. Furthermore, field data suggested that ponds in a New England salt marsh are isolated from the tidal
279 network and do not import sediment (Spivak et al., 2017). Overall, sediment deposition in the ponds is
280 likely very small, and for simplicity is set equal to zero.

281 The creep flux F parameterizes all processes that cause soil diffusion and is set equal to $\mu\nabla z$, where μ is
282 the soil diffusivity coefficient, whose value was empirically found equal to ~ 0.1 m²/yr (Mariotti et al.,
283 2019). The creep flux is set equal to zero within ponds and, more importantly, at the pond edges. This
284 choice reflects the absence of tidal oscillations, a process that creates “tidal fatigue” and is responsible for
285 the fast creep in channel banks (Mariotti et al., 2019). This is due to the standing water in the isolated
286 ponds maintaining hydrostatic pressure on the pond bank and preventing slumping during low tide. Thus,
287 the model allows isolated ponds to have relatively steep banks, as observed in the field (Wilson et al.,
288 2010). When pond cells reconnect, they drain instantaneously, and creep can take place. Excluding the
289 creep process at the edge of isolated ponds results in isolated pond expansion only occurring according to
290 the pond expansion term k_{exp} , which can be calibrated by direct comparison with the observed historical
291 expansion rate of isolated ponds. To summarize, creep does not affect isolated pond dynamics, but does
292 affect the dynamics of mudflats (i.e., connected ponds) and prevents the formation of an unrealistically
293 large elevation gradient in the marsh interior, which in reality might have been smoothed by
294 hydrodynamic processes other than creep but that the model is unable to explicitly simulate.

295 The channel dynamics is not explicitly simulated, and the channel elevation is kept equal to the lower
296 limit for vegetation growth. This elevation acts as a boundary condition for the bed elevation gradients

297 and thus affects the sediment creep flux near the banks. Noticeably, creep from the marsh platform into
298 the channels moves material out of the marsh domain and thus acts as a sink. Creep can also redistribute
299 sediment within the marsh domain; this does not count as either a sink or source because it conserves
300 sediment.

301 Finally, the term P includes the platform elevation loss through pond processes. When a connected cell
302 becomes a pond cell by either pond formation or pond expansion, it loses the elevation $Y = \min(Y_{max},$
303 $\max(0, z - z_{min}))$, where Y_{max} is the maximum scour thickness, calibrated with field data, and z_{min} is the
304 lower elevation limit below which pond scour does not occur. Y is the thickness of the material that is
305 instantaneously removed from the system, such that the elevation z is lowered by the amount Y .

306 The term P also includes pond deepening, which simulates organic matter decomposition via sulfate
307 reduction in the bed of the pond. Pond deepening is set equal to a constant rate ($P_{deepening}$) if $z > z_{min}$ and to
308 zero if $z < z_{min}$. Even though we introduced active pond deepening to simulate the loss of elevation caused
309 by organic matter decomposition, this term could be more generally considered as the net effect of all the
310 processes that change pond elevation. For example, if we assume that some sediment settles in the pond
311 during high tide, the term $P_{deepening}$ should be interpreted as the net deepening, including the actual pond
312 deepening by organic matter decomposition minus the elevation gain caused by sediment deposition. If
313 sediment deposition was larger than organic matter decomposition, $P_{deepening}$ could be negative, and the
314 pond might gain elevation through time. Given that this parameter is calibrated by comparing measured
315 and modeled pond depths, not by directly measuring the deepening or accretion, we are unable to isolate
316 these two components.

317 To summarize, the pond depth, relative to the surrounding marsh platform, is controlled by three
318 mechanisms: 1) the initial scour, which takes place by either pond formation or expansion, 2) the active
319 pond deepening, and 3) the relative deepening caused by the surrounding marsh gaining elevation through
320 organic and inorganic accretion.

321 **3.4 Coupling between pond dynamics and elevation dynamics**

322 As outlined above, the bed elevation is affected by pond processes of formation, expansion, and
323 deepening through the term P (Eq. 1). While the cellular automata model formulated in Section 2.2 is
324 independent of bed elevation, the elevation dynamics is introduced by allowing ponds to form and expand
325 only in vegetated marsh cells. This rule keeps ponds from forming and expanding into a mudflat, which is
326 defined as a connected cell with an elevation lower than z_{min} . This model implementation is a result of
327 only allowing the processes associated with isolated pond formation and expansion to occur in highly
328 organic soil that can be oxidized and compressed.

329 If the pond elevation at the time of drainage is higher than z_{min} , the pond revegetates just after it is
330 drained. In other words, the cell instantaneously switches from a pond to a vegetated marsh status. In this
331 scenario, every cell that is not a pond is a vegetated marsh that can be transformed back to a pond through
332 either pond formation or pond expansion. In this case, the pond dynamics without elevation is equivalent
333 to the pond dynamics with elevation, so the cellular automata can be run independently of the elevation.

334 On the other hand, if the connected ponds do not revegetate immediately, they become mudflat cells in
335 which ponds are not allowed to form (because $z < z_{min}$). These areas affect the dynamics of pond formation
336 and expansion, and thus the cellular automata model needs to be run together with the elevation model.

337 A special consideration should be given to cells whose elevation drops below the vegetation limit z_{min} .
338 These cells can be either drowned ponds or mudflats (Fig. 2). Neither has organic accretion by vegetation
339 (Eq. 3), but only the mudflat cells receive inorganic sediment and are allowed to creep under the model
340 specifications. If a drowned pond is surrounded by mudflats, the pond cannot expand. As a result,
341 drowned ponds will never intercept a channel and will never drain in the model domain. In reality,
342 drowned ponds should connect to the channel network through channels that quickly form in the
343 mudflats, but these are not explicitly simulated in the model. Connecting these drowned ponds to creeks
344 will not immediately allow for pond revegetation since the pond is still below the vegetation limit, but it
345 will allow for inorganic accretion and creep, which will both increase the bed elevation and potentially
346 allow for revegetation. In the model we account for this dynamic by introducing the rule that any drowned

347 pond that touches a mudflat becomes a mudflat itself, and receives inorganic sediment. Then, the
348 evolution of the mudflat would follow the elevation dynamics as previously described.

349 To summarize, the pond dynamics can be affected by the presence of mudflat cells, since ponds cannot
350 form or expand into these cells. The formation of mudflats is controlled by active pond deepening
351 ($P_{deepening}$) and by RSLR; the recovery of mudflats is controlled by mud accumulation and by RSLR (Fig.
352 2). If the amount of mudflats at any time is negligible (a few percent of the total marsh area), then the
353 elevation dynamics would in practice not affect the pond dynamics.

354 **4. Results**

355 **4.1 Field measurements**

356 The pond expansion rate, calculated using remote sensing, was equal to ~ 1.5 cm/yr, with a weak
357 dependence on the pond size (Fig. 3). This is calculated for ponds that did not merge between 1973 and
358 2014 and thus only includes ponds smaller than about 20 m. We were not able to measure expansion for
359 larger ponds. Detailed transects across thirteen ponds indicate that ponds are 0.3-1.2 m deep and that their
360 depth increases with diameter. The survey of 200 marsh-pond boundaries revealed that the depth of the
361 pond immediately adjacent to the bank was 0.46 ± 0.21 m. As such, the depth of the pond close to the edge
362 is relatively uniform, whereas the depth in the middle of the pond has a greater variability. Field
363 measurements at Barnstable marsh show an accretion of 4.6 ± 2.5 mm/yr near the channel and 5.1 ± 3.3
364 mm/yr in the marsh interior over the past 100 years (Table 1). Total suspended sediment concentrations
365 were 29.3 ± 3.6 mg/l for Barnstable and 5.0 ± 2.8 mg/l for Sage Lot pond.

366 **4.2 Pond dynamics not coupled to elevation**

367 The model simulations were run in a portion of the Barnstable marsh about 1.2 x 1.2 km (Fig. 1C). Using
368 the 2014 Lidar topography, the channel network was defined as the area with an elevation lower than the
369 limit for vegetation growth, which was assumed to be equal to MSL. Areas that were identified as ponds
370 (Section 2.1) were excluded from the channel network.

371 The pond model is first run without including the requirement that ponds can only form and expand
372 where the marsh elevation is greater than z_{min} . In this case, the pond dynamics does not depend on bed
373 elevation. This simplification is equivalent to the fully coupled model if the pond elevation never drops
374 below z_{min} , and it is nearly equivalent to the fully coupled model if the amount of mudflats is negligible,
375 which is the case if mudflats recover quickly. The advantage of running the model without the elevation
376 dynamics is to emphasize a key feature of pond dynamics, that is, the spatial distribution of ponds does
377 not depend on RSLR and sediment supply. As such, the parameters for pond evolution (k_{seed} and k_{exp}) can
378 be calibrated against observations without being affected by the uncertainties associated with RSLR (and
379 its variability during the last century) and sediment supply (which is estimated using a limited number of
380 samples).

381 Starting with a marsh without ponds, we run the model for 1000 years to reach a steady state, defined as
382 the period in which the time-averaged statistical distribution of ponds does not change. We found that
383 pond dynamics does not depend on the size of the ponds formed via the seeding mechanism, rather the
384 same steady state pond distribution is obtained if the ponds formed by the seeding mechanism are
385 composed of a single or several cells (and thus the initial ponds is larger). This occurs because the amount
386 of pond area created by seeding, where ponds are introduced into the model, is small compared to the area
387 gained by pond expansion. As such, the main effect of pond formation is not to directly increase the pond
388 area, but rather to create “seeds” that allow for pond expansion. This also confirms that pond formation
389 should have units of #ponds·m²·yr⁻¹ and not of m²·m²·yr⁻¹.

390 We found that the steady state pond size distribution only depends on the ratio between pond formation
391 and expansion rates. This is confirmed by noticing that the ratio between the two rates has units of
392 #ponds/m³ and is independent of time. The actual values of the rates only affect the time needed to reach
393 the steady state distribution. The ratio between pond formation and expansion rate that best fits the pond
394 size distribution (Fig. 4) is 0.027 #ponds/m³. If the ratio decreases, the number of small ponds decreases
395 while allowing for only a few large ponds (Fig. 4). Intuitively, in this scenario each pond has more time to

396 expand before eventually being drained. Using the measured pond expansion rate (1.5 cm/yr), the pond
397 formation rate is estimated to be $4 \cdot 10^{-4}$ ponds \cdot m² \cdot yr⁻¹. We could not directly measure this rate because of
398 the difficulty of detecting small ponds.

399 **4.3 Elevation dynamics**

400 Simulations that include the elevation dynamics (Section 2.3) are run for 1000 years, in which the first
401 900 years have R of 1 mm/yr and the last 100 years have R of 2.9 mm/yr, thus representing the RSLR
402 acceleration in the 19th century (NOAA Woods Hole Station 8447930). Thus, year 900 of the simulation
403 roughly corresponds to year 1914, whereas year 1000 roughly corresponds to year 2014 (i.e., present
404 time). The model at year 0 is initialized with an elevation equal to the 90th percentile of the vegetation
405 range, i.e., $0.9(r/2)=1.62$ m. Despite this initialization of marsh elevation being arbitrary, it does not affect
406 the results after about 500 years. Put differently, any initial marsh elevation would lead to the
407 (statistically) same results during the last few hundred years of the simulation. As such, this approach
408 recreates a synthetic marsh representative for the beginning of the 20th century that is 1) at steady state
409 according to the processes included in the model, 2) independent of any arbitrary initial marsh elevation,
410 3) independent of any topography measured at present time. Specifically, the measured Lidar is not used
411 to initialize the marsh elevation nor the pond distribution. Only the geospatial distribution of channels
412 (which could be reconstructed from aerial images without elevation) is needed to initialize the model.

413 First, we consider the elevation dynamics without the presence of ponds (Fig. 5). We analyze this
414 scenario by considering the spatially averaged vertical fluxes over the marsh domain (Fig. 6). As
415 expected, the net vertical accretion is equal to the RSLR rate. When RSLR rate increases to 2.9 mm/yr,
416 the net vertical accretion lags behind, but it nearly matches the RSLR rate after about 100 years (i.e., at
417 present times). The gross vertical accretion at present times is 5.1 mm/yr. This value represents the
418 spatially averaged accretion rate; in reality the accretion is much higher in the marsh adjacent (<10 m) to
419 channels, where it can be up to 20 mm/yr (Figs. 5, 7C). This additional accretion is balanced by bank
420 creep, which transports sediment out of the marsh domain. When spatially averaged over the entire marsh,

421 this creep flux creates an equivalent deficit of 2.2 mm/yr, which allows the net vertical accretion to
422 balance the RSLR rate (Fig. 6).

423 Next, we run the model including the mechanisms of pond formation, expansion, and deepening. The
424 maximum initial pond depth Y_{max} (which is both the maximum initial scour of new ponds, as well as the
425 maximum initial scour when the pond edge expands) is set equal to the measured height of the pond edge,
426 which was measured for Barnstable marsh to be 0.46 m. The consequences of this choice in the model are
427 that 1) small ponds would have a nearly uniform depth across the pond, and that depth would be about
428 0.46 m, 2) larger ponds would have a depth greater than 0.46 m in their center, which is older and thus
429 may have deepened over time due to organic matter decomposition as well as accretion of the adjacent
430 marsh platform, whereas their edges, which formed recently, would have a depth of ~0.46 m. The active
431 pond deepening $P_{deepening}$ was instead calibrated to match the observed depth in the middle of the ponds
432 (Fig. 8). As expected, the pond depth is much greater in the middle than at the edge, and the depth in the
433 middle of the pond increases with the pond diameter.

434 Ponds do not affect the marsh dynamics in the buffer zone close to the channel network, where ponds are
435 drained instantaneously. This is equivalent to assuming that they do not form at all and cannot expand. As
436 such, the model that includes pond dynamics has a similar pattern of bank creep and excess accretion on
437 the marsh adjacent to the channel as the model without pond dynamics (Fig. 6). On the other hand, ponds
438 drastically change the dynamics of the marsh interior. Ponding creates a heterogeneous landscape, with
439 low elevation areas surrounded by high marsh areas. This elevation pattern is mirrored by a spatially
440 heterogeneous vertical accretion, where the net vertical accretion in ponds is zero (if not negative,
441 because of active pond deepening), whereas recently connected ponds experience enhanced vertical
442 accretion. Compared to the case without ponds, the average marsh elevation is also lower.

443 Because pond reconnection is a stochastic process, the vertical accretion rate is not constant in time. In
444 particular, there are periods when large ponds are drained and the vertical accretion suddenly increases
445 (Fig. 6). Over a sufficient time period (e.g. 50 years), however, the net vertical accretion rate is equal to R .

446 **4.4 Exploring the effects of RSLR rate, sediment supply, and tidal range**

447 To generalize our results, we perform a series of explorative simulations with different sediment supplies
448 (C_o), RSLR rates (R), and tidal ranges (r). In order to consistently initialize the simulations, we start with
449 a uniform elevation equal to $0.9(r/2)$ with no ponds, and then run the model with R equal to 1 mm/yr for
450 500 years, which is enough to establish a steady state pond distribution (Fig. 6). As already pointed out,
451 the choice of the initial elevation does not affect the results after about 500 years. After 500 years, we
452 changed a single parameter (either R or C_o) while keeping all the other parameters fixed, and run the
453 simulations for an additional 1000 years (Fig. 9). We focused on scenarios in which the vegetated marsh
454 kept pace with RSLR and thus all marsh loss is due to pond expansion.

455 First, we consider the effects on increasing R or decreasing C_o in a mesotidal marsh such as Barnstable
456 marsh. For the relatively high sediment supply of Barnstable marsh ($C_o=30$ mg/l), the RSLR rate does not
457 affect the dynamics of ponds, which always occupies $\sim 10\%$ of the marsh. For the case with a lower $C_o=10$
458 mg/l, lower R gives nearly identical results as for the case with a higher C_o , with pond area remaining at
459 $\sim 10\%$ of the total marsh area, whereas high R starts to affect pond area (Fig. 9A). For example, for $C_o=10$
460 mg/l and $R=8$ mm/yr, the total unvegetated area (ponds plus mudflats) increases to about 25% within 500
461 years (Fig. 9A). Noticeably, under these conditions, the unvegetated area stabilizes and does not increase
462 indefinitely even after 1000 years.

463 Next, we consider the case of a marsh with a smaller tidal range. We use as a reference Sage Lot Pond
464 marsh, which has a spring tidal range of 0.7 m ([Gonneea et al. 2019](#)). Field measurements indicate that
465 this marsh has a small sediment supply equal to 5 mg/l. For simplicity, we consider the same channel
466 geometry as of Barnstable marsh but with a smaller tidal range. Accordingly, we modify the vegetation
467 limit, the initial marsh elevation, the maximum initial pond elevation, and the spring-neap variability
468 (Table 2). For the microtidal case, we found that for low R the unvegetated area is still $\sim 10\%$, but for
469 higher rates the unvegetated area increases quickly, and can be up to 100%, indicating loss of the entire

470 the marsh platform (Fig. 9B). The model predicts that the marsh would enter the pond runaway regime for
471 $R \sim 3$ mm/yr (Fig. 9B).

472 We also compared the model predictions with the measured accretion rates in Barnstable and Sage Lot
473 Pond marsh. We separated the spatially averaged accretion predicted by the model between the marsh
474 adjacent to channels (less than 10 m from the nearest channel, which roughly coincides with the low
475 marsh, and is about 29% of the total marsh area) and the marsh interior (more than 10 m from the nearest
476 channel, where bank creep is virtually zero, and is about 71% of the total marsh area). For a marsh with
477 low tidal amplitude and sediment supply such as Sage Lot Pond, the model predicts that when RSLR rate
478 was 1 mm/yr, the gross vertical accretion rates was ~ 2.6 mm/yr in the marsh adjacent to channels and
479 ~ 1.4 mm/yr for the marsh interior (Fig. 7B). After the acceleration in RSLR to 2.9 mm/yr the model
480 predicts that the gross vertical accretion increases to ~ 4.1 mm/yr in the marsh adjacent to the channels and
481 to ~ 3 mm/yr in the marsh interior (Fig. 7B). For comparison, the field measurements of accretion over a
482 100 year period, which includes the period during modern RSLR acceleration, indicate an accretion rate
483 of 3.7 ± 2.0 mm/yr close to the channels and 1.4 ± 0.3 mm/yr in the interior (Table 1). For the Barnstable
484 marsh, with a higher tidal range and sediment supply, the model predicts gross vertical accretion rates of
485 ~ 9.5 mm/yr near channels and ~ 2.8 mm/year in the marsh interior when RSLR rate is 1 mm/yr, and ~ 11.5
486 mm/yr near channels and ~ 4.0 mm/year in the marsh interior when RSLR rate is 2.9 mm/yr (Fig. 7A). For
487 comparison, field measurements at Barnstable marsh show an accretion of 4.6 ± 2.5 mm/yr near the
488 channel and 5.1 ± 3.3 mm/yr in the marsh interior over the past 100 years.

489 As an indicator of the overall marsh status, we calculated the spatially-averaged primary productivity
490 normalized by the maximum productivity (Fig. 9). The productivity of the vegetated marsh depends on
491 the bed elevation following the function B (section 3.3), whereas the productivity in the ponds is equal to
492 zero. As the RSLR rate increases, the marsh elevation decreases and thus the productivity increases. As
493 the unvegetated pond area starts to increase, however, the overall marsh productivity starts to decrease.
494 This is particularly evident for the Sage Lot Pond marsh for a RSLR rate greater than 4 mm/yr (Fig. 9B).

495 Finally, we expanded these simulations by systematically considering different tidal ranges (0.7, 1.6, 3.6
496 m), RSLR rates (1 to 8 mm/yr), and sediment supply concentrations (5 to 30 mg/l) (Fig. 10). We found
497 that, for small tidal ranges, the rate of marsh loss by pond expansion is highly sensitive to the RSLR rate.
498 When the RSLR rate increases to 3 mm/yr, marsh loss occurs but is relatively slow, and the amount of
499 unvegetated area (which includes both ponds and mudflats) increases from 10% to 15% of the total marsh
500 area during the first 100 years (Fig. 9). A further increase in the RSLR rate (5 mm/yr) drastically
501 increases the rate of marsh loss, with the amount of unvegetated area increasing from 10% to 40% of the
502 total marsh area during the first 100 years.

503 **5. Discussion**

504 **5.1 The pervasive effect of ponds in salt marshes**

505 Ponds in Barnstable marsh expand at a very slow rate (1.5 cm/yr) compared to exposed marsh creekbank
506 edges that retreat by wave-induced erosion (0.5-10 m/yr) (Elsey-Quirk et al., 2019; Hopkinson et al.,
507 2018; Leonardi et al., 2016; Marani et al., 2011). Yet, ponds are numerous and collectively have a long
508 perimeter, and thus are able to affect nearly the entire marsh surface on millennial time scales.
509 Considering an average unchanneled length of 50 m (Marani et al., 2003), a pond formed in the middle of
510 the marsh would take ~2000 years to reach an area influenced by channel network and drain. Since some
511 ponds form closer to the channel network initially, 2000 years is likely an upper estimate of the time
512 needed to reconnect ponds to the channel network and drain. In addition, ponds that merge together will
513 drastically reduce the time needed for a pond to reconnect to the channel network.
514 Given that the Barnstable marsh is ~4000 years old (Redfield, 1965), we expect that any point on the
515 marsh was at least once a pond. Indeed, stratigraphic evidence of ponds were found in nearly all cores
516 taken in a New England salt marsh (ME, USA) (Wilson et al., 2009). However, many historical records
517 within salt marshes only extend ~100 years, due to age model constraints of the commonly used lead-210
518 methods, and thus may miss some of these millennial scale dynamics. In any case, the assumption of
519 steady state marsh accretion often used while interpreting the sedimentary record (Morris et al., 2016)

520 should be evaluated, since even if RLSR rate and sediment supply are constant, a specific site within the
521 marsh may not be at steady state at any given time due to pond dynamics.

522 Another consequence of pond dynamics is that recently connected ponds (as identified in Fig. 1E) are a
523 common feature and should be interpreted as part of the basic marsh dynamics as opposed to an indicator
524 of changes in boundary conditions. Thus, ponds do not necessarily indicate an acceleration in RSLR or
525 other anthropogenic modifications, but are rather a natural occurrence within many salt marshes. Ponds
526 also create diverse habitats and ecological niches for wildlife (Brush et al., 1986), and thus should not
527 necessarily be considered a negative feature within salt marshes.

528 **5.2 Vertical accretion in the pond recovery regime**

529 When the marsh is in the pond recovery regime, pond dynamics in the marsh interior increased the
530 spatially-averaged gross vertical accretion by 0.5-2 mm/yr (Fig. 7), a result that was previously predicted
531 (Kirwan et al., 2008). This excess accretion is larger for larger tidal ranges, because marshes with a larger
532 tidal range have a thicker soil profile that can be removed by the ponding processes. Ponding also results
533 in highly heterogeneous accretion across the marsh platform (Fig. 5), and thus the excess accretion rate
534 during pond recovery could locally be much higher than 2 mm/yr. For example, the model predicts that
535 recovering ponds might have accretion rates up to 20 mm/yr (Fig. 5). Indeed, Wilson et al., (2014)
536 reported vertical accretion rates of 8 mm/yr in recently recovered ponds in a New England salt marsh,
537 despite the fact that the sediment supply in that marsh was extremely low (~5 mg/l). The model predicts
538 that the excess accretion rate persists from when a pond revegetates until it reaches the equilibrium
539 elevation with the marsh surface. In other words, ponds that were drained centuries ago might not have
540 fully equilibrated and thus might still accrete slightly faster than the RSLR rate. These predictions are
541 consistent with the 5.1 mm/yr vertical accretion measured in the marsh interior of Barnstable marsh
542 during a period when relative sea-level rise rate was 2.9 mm/y (NOAA Woods Hole Station 8447930)
543 (Table 1).

544 Our model also predicts channel bank creep causes an equivalent elevation drop of ~ 2 mm/yr when
545 averaged over the whole marsh platform (Fig. 6,7). This loss is balanced by an excess vertical accretion
546 (Mariotti et al., 2016), which can be observed by the gross vertical accretion rate being much larger than
547 the RSLR rate. Contrary to ponding, this bank creep is localized to the low marsh immediately adjacent to
548 channels, where the excess vertical accretion can be an order of magnitude higher than RSLR rate (i.e., up
549 to 20 mm/yr, Fig. 5). This prediction is consistent with the larger vertical accretion rates measured on the
550 marsh adjacent to channels than on the marsh interior at Sage Lot Pond marsh (Table 1). For Barnstable
551 marsh, the model predicts that the vertical accretion on the marsh adjacent to channels is ~ 11 mm/yr (Fig.
552 7A), which is much larger than the measured 4.6 ± 2.5 mm/yr (Table 1). One possible explanation is that
553 the channel-adjacent area in the model integrates portions of the marsh that are extremely low (e.g., the
554 vegetated bank located a few meters from the channel). These low areas have a disproportionately high
555 excess accretion (Fig. 5 and Fig. 7C,D) and strongly influence the average value over the area here
556 defined as channel-adjacent (< 10 m from the channel network). Field measurements in the channel-
557 adjacent area, in contrast, are generally taken a few meters inland from the edge of the marsh, with a
558 higher elevation than the slumping blocks and where the excess accretion is much lower. Indeed, the
559 cores in Barnstable collected ~ 2 m from the marsh edge are actually ~ 5 m from the lowest vegetated point
560 (Fig. 1H). Noticeably, the model predicts a minimum in vertical accretion, equal to about 3 mm/yr,
561 located between 5 and 20 m from the channel (Fig. 7C). This is the region where neither bank creep nor
562 ponding are present, and thus the gross accretion rate matches RSLR rate.

563 The model also recreates the lagged vertical accretion that follows the acceleration in RSLR rate, a
564 disequilibrium effect has been previously identified with simplified marsh models (Kirwan and
565 Temmerman, 2009; Kirwan and Murray, 2008). This lag should be present in every salt marsh that
566 experienced accelerated RSLR, regardless of pond occurrence or the influence of bank creep.

567 To summarize, the model is able to combine three previously identified mechanisms by which vertical
568 accretion rates deviate from the RSLR rate, emphasizing that a direct comparison between vertical

569 accretion and RSLR rate can be misleading at best, and overly optimistic for projecting marsh elevation
570 trajectories.

571 **5.3 Vertical accretion in the pond runaway regime**

572 The simple lumped model (Mariotti, 2016) identified the minimum unvegetated accretion,
573 $D_{cr}=C\cdot r/(2T\cdot\rho_m)$, as the threshold between pond recovery and pond runaway regimes. Because C is not
574 spatially uniform, D_{cr} varies among the domain. D_{cr} is lowest in the marsh interior, where
575 $D_{cr}=\alpha\cdot C_o\cdot r/(2T\cdot\rho_m)$.

576 For $R<D_{cr}$, the lumped pond model predicts that every pond recovers. Indeed, the spatially explicit model
577 predicts that, for any RSLR rate lower than D_{cr} , ponds always occupy ~10% of the marsh area (Figs.
578 9,10). This prediction agrees with the finding that stable salt marshes are associated with an unvegetated-
579 vegetated ratio of ~0.1 (Wasson et al., 2019) (a pond area of 10% corresponds to an unvegetated-
580 vegetated ratio of 0.11). As for the lumped model, the spatially explicit model predicts an increase in the
581 total unvegetated area as $R>D_{cr}$. The spatially explicit model provides more information than the lumped
582 model, and specifically predicts that the rate at which marsh loss by pond expansion takes place strongly
583 increases as R further exceeds D_{cr} . Put differently, when R is just slightly above D_{cr} , the rate of marsh loss
584 by pond expansion is extremely low, and the marsh could last thousands of years. On the other hand, once
585 the threshold for pond runaway is exceeded, even small increases in R could have catastrophic
586 consequences for marsh loss.

587 Using D_{cr} as the threshold for the pond runaway regime is further complicated by the presence of creep,
588 which can take place at the edge of mudflats (i.e., connected ponds). Creep transfers sediment from high
589 to low elevations, and thus tends to increase vertical accretion in the mudflats and to lower vertical
590 accretion on the vegetated platform. For example, a very small mudflat might recover even if R is slightly
591 larger than D_{cr} (which explains why the Sage Lot Pond marsh does not enter the pond runaway regime for
592 $R=1$ mm/yr even if $D_{cr}=0.6$ mm/yr). Lateral transport of sediment not associated with creep, including
593 sediment transport by waves or sheet flow over the marsh, might slightly alter the predictions purely

594 based on vertical accretion rates. Nonetheless, the parameter D_{cr} captures the transition to the pond
595 runaway regime within an uncertainty of about 1 mm/yr (Fig. 10).

596 **5.4 Pond formation**

597 A crucial parameter in the model is the rate of pond formation. If ponds do not form, neither the pond
598 recovery nor the pond runaway regime occurs. In this case, the marsh is either fully vegetated or
599 disappears by drowning, and thus the marsh landscape is dramatically different than what simulated in our
600 model (Fig. 5). As such, it is noteworthy to emphasize that ponds are not always present in salt marshes.
601 Ponds have been identified in the Mid-Atlantic and New England Coast of the USA (Adamowicz and
602 Roman, 2005; Mariotti, 2016; Schepers et al., 2017) as well as in the northern Gulf of Mexico (Mariotti,
603 2016; Nyman et al., 1994). Yet, marshes in the South-Atlantic Coast of the USA, including sites with
604 relatively little human modifications such as in Virginia and Georgia, seem to have few ponds if any at
605 all. For marshes in which ponds are not common, it is possible that either ponds do not form at all or that
606 the pond formation rate (the parameter k_{seed}) is extremely low. In this latter case the model would predict
607 that the number of ponds would be highly reduced (Fig. 4) and that their size distribution would be highly
608 skewed towards a few large ponds.

609 In this study, we assumed that ponds form without explicitly simulating the mechanisms that lead to pond
610 formation in the first place. In particular, we did not investigate whether the rate of pond formation
611 changes as a function of environmental drivers. We can only speculate that pond formation might be
612 related to disturbances related to climate via ice rafting and scour, excessive wrack accumulation,
613 grazing/bioturbation such as by *Sesarma reticulatum* crab or burrowing species such as fiddler crabs (*Uca*
614 sp.), and to biogeochemical and hydrological processes associated with microtopography.

615 We further emphasize that pond formation *per se* is not directly driving permanent marsh loss, but it
616 could lead to marsh loss in the pond runaway regime. In the pond runaway regime, an increase in the
617 pond formation rate would directly increase the rate at which the marsh is lost, mainly by increasing the
618 “seeds” from which ponds can expand. Pond formation is thus an example of a relatively secondary

619 mechanism that, through spatial interactions (Larsen, 2019), could lead to rapid marsh loss. Thus, we
620 argue that future research should develop a mechanistic understanding of pond formation and determine
621 whether environmental changes such climate or burrowing and grazing pressure, might increase the rate
622 of pond formation.

623 **5.5 Marsh management**

624 All simulations were performed for scenarios in which the vegetated marsh keeps pace with RSLR. As
625 such, if pond dynamics were not included, the marsh would have been preserved indefinitely and there
626 would have not been any unvegetated area occupied by either ponds or mudflats. Thus, including pond
627 dynamics in marshes where ponds are known to form is an essential step to simulate marsh evolution.

628 Including pond dynamics in marsh models is also essential for predicting ecosystem productivity. Marsh
629 grasses remove CO₂ from the atmosphere and bury it in soils, support coastal food webs, and filter
630 inorganic nutrients washed from the landscape, among other ecosystem services. As such, changes in
631 productivity have consequences for ecological and biogeochemical processes within marshes and adjacent
632 ecosystems. In both the mesotidal (Barnstable) and microtidal (Sage Lot Pond) simulations, normalized
633 primary productivity increases monotonically with the RSLR rate (Fig. 9). The expansion of the
634 unvegetated area for very high RSLR rates, however, starts to decrease productivity. For the microtidal
635 case, a decrease in productivity associated with pond expansion could be observed even at the decadal
636 time scale (Fig. 9B), and thus could be relevant for coastal management.

637 As previously identified (Mariotti, 2016), neither the presence of ponds nor the expansion of ponds is a
638 sign of permanent marsh loss. On the other hand, the absence of pond recovery is a potential indicator of
639 a regime shift. Monitoring pond recovery, such as by measuring their accretion rates once reconnected to
640 the channel network, should thus become a routine marsh assessment, alongside measurements of vertical
641 accretion in the vegetated marsh.

642 One management question is whether to promote or prevent pond recovery. One example includes
643 selectively digging ditches to reconnect ponds, a strategy referred to as “quality ditching” or Open Water
644 Marsh Management (Wolfe, 1996). Our model suggests that the appropriate management (in terms of
645 morphological evolution of the salt marsh) depends on whether the marsh is in the pond recovery or pond
646 runaway regime. In the former case, favoring pond drainage should accelerate vertical accretion, in the
647 latter it would accelerate marsh loss.

648 As previously shown in a model that only considers one pond (Mariotti, 2016), determining whether a
649 marsh is in the pond runaway or pond recovery regimes requires an estimate of the minimum inorganic
650 deposition in the marsh interior (D_{cr}), and specifically to estimate the suspended sediment concentration.
651 Because this parameter is difficult to determine without long-term monitoring (Ganju et al., 2017), we
652 suggest that analyzing the trajectory of recently connected ponds is important to determine whether ponds
653 are recovering or expanding indefinitely.

654 **5.6 Model limitations and future directions**

655 The model assumes that any connected area above z_{min} revegetates instantaneously. Therefore, a mudflat
656 is only present if $z < z_{min}$. In reality it could take several years for a connected pond to revegetate even if
657 $z > z_{min}$. For example, the recently connected ponds in Barnstable have not fully revegetated even if their
658 elevation is ~ 1 m above MSL (i.e., $z > z_{min}$). Even though this delay could be included in the dynamics, we
659 argue that it is not crucial, because revegetation likely will occur within shorter times scales (decades)
660 than the time scale considered in this study. More importantly, large vertical accretion rates by mud
661 deposition could take place even though recently connected ponds are not fully revegetated.

662 Channels are assumed to be fixed. When analyzing historical imagery (~ 50 years), channels in Barnstable
663 marsh are relatively stable, even though they could have migrated over longer time scales. Migrating
664 channels would likely increase the rate at which ponds are intercepted and thus drained. Channel
665 migration could be parameterized as a larger value for the reference drainage distance L , allowing ponds
666 within the model to drain even if located at a large distance from channels. Indeed, this could be a

667 dominant mechanism for pond drainage at sites where channel migration is relatively fast (Finotello et al.,
668 2018). Channel migration would likely result in similar marsh evolution dynamics and pond recovery,
669 with marsh loss at the eroding bank but, at the same time, induce accretion that is faster than the RSRL
670 rate at the accreting bank.

671 The model does not conserve sediment in the channel domain: the sediment transported from the bank to
672 the channel through the creep mechanism does not accumulate in the channel, and the sediment
673 transported from the channel to the marsh, which is responsible for the term D_m , does not cause a
674 sediment deficit in the channel network. That is, we assume that there is an infinite supply of new
675 sediment from the channels. In reality, a portion of the bank material that creeps into the channel would
676 be resuspended and re-transported to the marsh platform, thus allowing for sediment recycling. This
677 component cannot be reproduced in the model, since an explicit representation of the channel dynamics
678 would be needed.

679 Finally, the model does not include the dynamics of hydrological alterations such as ditching, which is a
680 common feature in New England salt marshes. Ditching could impact the marsh elevation dynamics in at
681 least two ways. On one hand, ditches could cause a nearly instantaneous marsh-wide pond drainage,
682 which could temporarily increase the spatially averaged vertical accretion rate. On the other hand, ditches
683 could lower the water table and cause a combination of carbon oxidation and compaction, which in turn
684 could lower the marsh elevation. Such effects could be included in the model by 1) allowing ponds close
685 to the ditches to be drained similarly to the ponds drained by the natural channel network, and 2) adding
686 an additional term in Eq. 1 to simulate a localized bed lowering close to the ditches.

687 **6. Conclusions**

688 The proposed model simulates the spatially explicit dynamics of marsh ponds, and thus allows simulation
689 of the aggregated effect that ponds have on the evolution of the marsh platform. The Barnstable marsh is
690 predicted to be in a pond recovery regime: pond expansion does not cause net marsh loss because they
691 recover the marsh elevation once drained. Even in the pond recovery regime, however, ponds drastically

692 affect the marsh elevation and vertical accretion. In particular, pond dynamics explain why marsh vertical
693 accretion, even away from channels, could be several times larger than the rate of RSLR, and also why
694 the accretion rate is highly variable in space.

695 The model predicts that future increases in RSLR rate at Barnstable marsh would not cause the marsh to
696 transition to the full pond runaway regime. Yet, with a large RSLR rate and a reduced sediment supply,
697 ponds in the marsh interior might become permanent mudflats and thus increase the unvegetated area to
698 ~20% of the total marsh. Monitoring of pond recovery, such as by measuring their accretion rates once
699 reconnected to the channel network, could be used as a landscape-level indicator of regime shifts.

700 Marshes with a smaller tidal range and sediment supply, such as Sage Lot Pond marsh, are more prone to
701 enter the pond runaway regime. For RSLR rates just above the critical threshold (e.g., 3 mm/yr), the rate
702 of marsh loss by pond expansion is still relatively low, and the marsh could take several centuries (if not
703 millennia) before completely disappearing. A further acceleration in RSLR rate (e.g., 5 mm/yr) would
704 drastically increase the rate at which the marsh is lost by pond expansion – which will take place even
705 though the vegetated marsh keeps pace with RSLR.

706 Future research needs include understanding the mechanism of pond formation, evaluating how
707 hydrological alterations such as ditching affects pond dynamics, and quantifying how pond dynamics
708 affect blue carbon accumulation and preservation.

709

710 **Acknowledgments**

711 We appreciate funding support for this work from Woods Hole Sea Grant (NA14OAR4170104 to ACS
712 and GM) and NOAA NSC (NA14NOS4190145 to ACS, GM, MEG, and MT), USGS Coastal & Marine
713 Geology Program, the USGS Land Change Science Program's LandCarbon program. We thank the
714 Waquoit Bay National Estuarine Research Reserve and Sandy Neck Beach Park for providing research
715 access. USGS staff including T. Wallace Brooks, Jennifer O'Keefe Suttles, Adrian Mann and Allyson

716 Boggess provided field and analytical support. Additional field support was provided by Claire Mayorga,
717 Kelsey Gosselin, Madelyn Francesconi, and Sam MicNichol. Any use of trade, firm or product names is
718 for descriptive purposes only and does not imply endorsement by the U.S. Government.

719

720 **References**

- 721 Adamowicz, S.C., Roman, C.T., 2005. New England salt marsh pools: A quantitative analysis of
722 geomorphic and geographic features. *Wetlands* 25, 279–288. <https://doi.org/10.1672/4>
- 723 Appleby, P.G., Oldfield, F., 1978. The calculation of lead-210 dates assuming a constant rate of supply of
724 unsupported ²¹⁰Pb to the sediment. *CATENA* 5, 1–8. <https://doi.org/10.1016/S0341->
725 8162(78)80002-2
- 726 Argow, B.A., FitzGerald, D.M., 2006. Winter processes on northern salt marshes: Evaluating the impact
727 of in-situ peat compaction due to ice loading, Wells, ME. *Estuar. Coast. Shelf Sci., Salt Marsh*
728 *Geomorphology: Physical and ecological effects on landform* 69, 360–369.
729 <https://doi.org/10.1016/j.ecss.2006.05.006>
- 730 Argow, B.A., Hughes, Z.J., FitzGerald, D.M., 2011. Ice raft formation, sediment load, and theoretical
731 potential for ice-rafted sediment influx on northern coastal wetlands. *Cont. Shelf Res.* 31, 1294–
732 1305. <https://doi.org/10.1016/j.csr.2011.05.004>
- 733 Binford, M.W., 1990. Calculation and uncertainty analysis of ²¹⁰Pb dates for PIRLA project lake
734 sediment cores. *J. Paleolimnol.* 3, 253–267. <https://doi.org/10.1007/BF00219461>
- 735 Brush, T., Lent, R.A., Hrubby, T., Harrington, B.A., Marshall, R.M., Montgomery, W.G., 1986. Habitat
736 Use by Salt Marsh Birds and Response to Open Marsh Water Management. *Colon. Waterbirds* 9,
737 189–195. <https://doi.org/10.2307/1521212>
- 738 Cavatorta, J.R., Johnston, M., Hopkinson, C., Valentine, V., 2003. Patterns of sedimentation in a salt
739 marsh-dominated estuary. *Biol. Bull.* 205, 239–241.
- 740 Christiansen, T., Wiberg, P.L., Milligan, T.G., 2000. Flow and Sediment Transport on a Tidal Salt Marsh
741 Surface. *Estuar. Coast. Shelf Sci.* 50, 315–331. <https://doi.org/10.1006/ecss.2000.0548>
- 742 Cutshall, N.H., Larsen, I.L., Olsen, C.R., 1983. Direct analysis of ²¹⁰Pb in sediment samples: Self-
743 absorption corrections. *Nucl. Instrum. Methods Phys. Res.* 206, 309–312.
744 [https://doi.org/10.1016/0167-5087\(83\)91273-5](https://doi.org/10.1016/0167-5087(83)91273-5)
- 745 Elsey-Quirk, T., Mariotti, G., Valentine, K., Raper, K., 2019. Retreating marsh shoreline creates hotspots
746 of high-marsh plant diversity. *Sci. Rep.* 9, 5795. <https://doi.org/10.1038/s41598-019-42119-8>
- 747 Fagherazzi, S., Kirwan, M.L., Mudd, S.M., Guntenspergen, G.R., Temmerman, S., D’Alpaos, A., Koppel,
748 J., Rybczyk, J.M., Reyes, E., Craft, C., others, 2012. Numerical models of salt marsh evolution:
749 Ecological, geomorphic, and climatic factors. *Rev. Geophys.* 50.
- 750 Finotello, A., Lanzoni, S., Ghinassi, M., Marani, M., Rinaldo, A., D’Alpaos, A., 2018. Field migration
751 rates of tidal meanders recapitulate fluvial morphodynamics. *Proc. Natl. Acad. Sci.* 115, 1463–
752 1468. <https://doi.org/10.1073/pnas.1711330115>
- 753 Ganju, N.K., Defne, Z., Kirwan, M.L., Fagherazzi, S., D’Alpaos, A., Carniello, L., 2017. Spatially
754 integrative metrics reveal hidden vulnerability of microtidal salt marshes. *Nat. Commun.* 8.
755 <https://doi.org/10.1038/ncomms14156>
- 756 Gonnee, M.E., Maio, C.V., Kroeger, K.D., Hawkes, A.D., Mora, J., Sullivan, R., Madsen, S., Buzard,
757 R.M., Cahill, N., Donnelly, J.P., 2019. Salt marsh ecosystem restructuring enhances elevation
758 resilience and carbon storage during accelerating relative sea-level rise. *Estuar. Coast. Shelf Sci.*
759 217, 56–68. <https://doi.org/10.1016/j.ecss.2018.11.003>

760 Gonneea, M.E., O’Keefe Suttles, J.A., Kroeger, K.D., 2018. Collection, analysis, and age-dating of
761 sediment cores from salt marshes on the south shore of Cape Cod, Massachusetts, from 2013
762 through 2014. US Geol. Surv. Data Release <https://doi.org/10.5066/F7H41QPP>.

763 Harshberger, J.W., 1909. The Vegetation of the Salt Marshes and of the Salt and Fresh Water Ponds of
764 Northern Coastal New Jersey. *Proc. Acad. Nat. Sci. Phila.* 61, 373–400.

765 Hopkinson, C.S., Morris, J.T., Fagherazzi, S., Wollheim, W.M., Raymond, P.A., 2018. Lateral Marsh
766 Edge Erosion as a Source of Sediments for Vertical Marsh Accretion. *J. Geophys. Res.*
767 *Biogeosciences* 123, 2444–2465. <https://doi.org/10.1029/2017JG004358>

768 Howes, N.C., FitzGerald, D.M., Hughes, Z.J., Georgiou, I.Y., Kulp, M.A., Miner, M.D., Smith, J.M.,
769 Barras, J.A., 2010. Hurricane-induced failure of low salinity wetlands. *Proc. Natl. Acad. Sci.* 107,
770 14014–14019. <https://doi.org/10.1073/pnas.0914582107>

771 Johnston, M.E., Cavatorta, J.R., Hopkinson, C.S., Valentine, V., 2003. Importance of metabolism in the
772 development of salt marsh ponds. *Biol. Bull.* 205, 248–249.

773 Kesel, R.H., Smith, J.S., 1978. Tidal creek and pan formation in intertidal salt marshes, Nigg Bay,
774 Scotland. *Scott. Geogr. Mag.* 94, 159–168. <https://doi.org/10.1080/00369227808736403>

775 Kirwan, M., Temmerman, S., 2009. Coastal marsh response to historical and future sea-level acceleration.
776 *Quat. Sci. Rev., Quaternary Ice Sheet-Ocean Interactions and Landscape Responses* 28, 1801–
777 1808. <https://doi.org/10.1016/j.quascirev.2009.02.022>

778 Kirwan, M.L., Murray, A.B., 2008. Tidal marshes as disequilibrium landscapes? Lags between
779 morphology and Holocene sea level change. *Geophys. Res. Lett.* 35, L24401.
780 <https://doi.org/10.1029/2008GL036050>

781 Kirwan, M.L., Murray, A.B., 2007. A coupled geomorphic and ecological model of tidal marsh evolution.
782 *Proc. Natl. Acad. Sci.* 104, 6118–6122. <https://doi.org/10.1073/pnas.0700958104>

783 Kirwan, M.L., Murray, A.B., Boyd, W.S., 2008. Temporary vegetation disturbance as an explanation for
784 permanent loss of tidal wetlands. *Geophys. Res. Lett.* 35, n/a–n/a.
785 <https://doi.org/10.1029/2007GL032681>

786 Koop-Jakobsen, K., Gutbrod, M.S., 2019. Shallow Salt Marsh Tidal Ponds—An Environment With
787 Extreme Oxygen Dynamics. *Front. Environ. Sci.* 7. <https://doi.org/10.3389/fenvs.2019.00137>

788 Larsen, L.G., 2019. Multiscale flow-vegetation-sediment feedbacks in low-gradient landscapes.
789 *Geomorphology* 334, 165–193. <https://doi.org/10.1016/j.geomorph.2019.03.009>

790 Leonardi, N., Ganju, N.K., Fagherazzi, S., 2016. A linear relationship between wave power and erosion
791 determines salt-marsh resilience to violent storms and hurricanes. *Proc. Natl. Acad. Sci.* 113, 64–
792 68.

793 Marani, M., Belluco, E., D’Alpaos, A., Defina, A., Lanzoni, S., Rinaldo, A., 2003. On the drainage
794 density of tidal networks. *Water Resour. Res.* 39, 1040. <https://doi.org/10.1029/2001WR001051>

795 Marani, M., D’Alpaos, A., Lanzoni, S., Santalucia, M., 2011. Understanding and predicting wave erosion
796 of marsh edges. *Geophys. Res. Lett.* 38, L21401. <https://doi.org/10.1029/2011GL048995>

797 Marani, M., Lio, C.D., D’Alpaos, A., 2013. Vegetation engineers marsh morphology through multiple
798 competing stable states. *Proc. Natl. Acad. Sci.* 201218327.
799 <https://doi.org/10.1073/pnas.1218327110>

800 Mariotti, G., 2018. Marsh channel morphological response to sea level rise and sediment supply. *Estuar.*
801 *Coast. Shelf Sci.* <https://doi.org/10.1016/j.ecss.2018.05.016>

802 Mariotti, G., 2016. Revisiting salt marsh resilience to sea level rise: Are ponds responsible for permanent
803 land loss? *J. Geophys. Res. Earth Surf.* 121, 1391–1407. <https://doi.org/10.1002/2016JF003900>

804 Mariotti, G., Canestrelli, A., 2017. Long-term morphodynamics of muddy backbarrier basins: Fill in or
805 empty out? *Water Resour. Res.* 53, 7029–7054. <https://doi.org/10.1002/2017WR020461>

806 Mariotti, G., Kearney, W., Fagherazzi, S., 2016. Soil creep in salt marshes. *Geology* 44, 459–462.

807 Mariotti, G., Kearney, W.S., Fagherazzi, S., 2019. Soil creep in a mesotidal salt marsh channel bank: Fast,
808 seasonal, and water table mediated. *Geomorphology* 334, 126–137.
809 <https://doi.org/10.1016/j.geomorph.2019.03.001>

810 McKee, K.L., Patrick, W.H., Jr., 1988. The relationship of smooth cordgrass (*Spartina Alterniflora*) to
811 tidal datums: A review. *Estuaries* 11, 143–151. <https://doi.org/10.2307/1351966>

812 Morris, J.T., Barber, D.C., Callaway, J.C., Chambers, R., Hagen, S.C., Hopkinson, C.S., Johnson, B.J.,
813 Megonigal, P., Neubauer, S.C., Troxler, T., Wigand, C., 2016. Contributions of organic and
814 inorganic matter to sediment volume and accretion in tidal wetlands at steady state. *Earths Future*
815 4, 110–121. <https://doi.org/10.1002/2015EF000334>

816 Morris, J.T., Sundareshwar, P.V., Nietch, C.T., Kjerfve, B., Cahoon, D.R., 2002. Responses of coastal
817 wetlands to rising sea level. *Ecology* 83, 2869–2877. <https://doi.org/10.2307/3072022>

818 Nyman, J.A., Carlross, M., Delaune, R.D., Patrick, W.H., 1994. Erosion rather than plant dieback as the
819 mechanism of marsh loss in an estuarine marsh. *Earth Surf. Process. Landf.* 19, 69–84.
820 <https://doi.org/10.1002/esp.3290190106>

821 OCM Partners, 2019. 2013–2014 U.S. Geological Survey CMGP LiDAR: Post Sandy (MA, NH,
822 RI), <https://inport.nmfs.noaa.gov/inport/item/49846>.

823 Pethick, J.S., 1974. The distribution of salt pans on tidal salt marshes. *J. Biogeogr.* 1, 57–62.
824 <https://doi.org/10.2307/3038068>

825 Redfield, A.C., 1972. Development of a New England Salt Marsh. *Ecol. Monogr.* 42, 201–237.
826 <https://doi.org/10.2307/1942263>

827 Redfield, A.C., 1965. Ontogeny of a Salt Marsh Estuary. *Science* 147, 50–55.
828 <https://doi.org/10.1126/science.147.3653.50>

829 Schepers, L., Kirwan, M., Guntenspergen, G., Temmerman, S., 2017. Spatio-temporal development of
830 vegetation die-off in a submerging coastal marsh. *Limnol. Oceanogr.* 62, 137–150.
831 <https://doi.org/10.1002/lno.10381>

832 Spivak, A.C., Gosselin, K., Howard, E., Mariotti, G., Forbrich, I., Stanley, R., Sylva, S.P., 2017. Shallow
833 ponds are heterogeneous habitats within a temperate salt marsh ecosystem. *J. Geophys. Res.*
834 *Biogeosciences* 122, 1371–1384. <https://doi.org/10.1002/2017JG003780>

835 Spivak, A.C., Gosselin, K.M., Sylva, S.P., 2018. Shallow ponds are biogeochemically distinct habitats in
836 salt marsh ecosystems. *Limnol. Oceanogr.* 63, 1622–1642. <https://doi.org/10.1002/lno.10797>

837 van Huissteden, J., van de Plassche, O., 1998. Sulphate reduction as a geomorphological agent in tidal
838 marshes (‘Great Marshes’ at Barnstable, Cape Cod, USA). *Earth Surf. Process. Landf.* 23, 223–
839 236. [https://doi.org/10.1002/\(SICI\)1096-9837\(199803\)23:3<223::AID-ESP843>3.0.CO;2-I](https://doi.org/10.1002/(SICI)1096-9837(199803)23:3<223::AID-ESP843>3.0.CO;2-I)

840 Wasson, K., Ganju, N.K., Defne, Z., Endris, C., Eelsey-Quirk, T., Thorne, K.M., Freeman, C.M.,
841 Guntenspergen, G., Nowacki, D.J., Raposa, K.B., 2019. Understanding tidal marsh trajectories:
842 evaluation of multiple indicators of marsh persistence. *Environ. Res. Lett.* 14, 124073.
843 <https://doi.org/10.1088/1748-9326/ab5a94>

844 Wilson, C.A., Hughes, Z.J., FitzGerald, D.M., Hopkinson, C., Valentine, V., Kolker, A.S., 2014.
845 Saltmarsh Pool and Tidal Creek Morphodynamics: Dynamic Equilibrium of Northern Latitude
846 Saltmarshes? *Geomorphology*. <https://doi.org/10.1016/j.geomorph.2014.01.002>

847 Wilson, K.R., Kelley, J.T., Croitoru, A., Dionne, M., Belknap, D.F., Steneck, R., 2009. Stratigraphic and
848 Ecophysical Characterizations of Salt Pools: Dynamic Landforms of the Webhannet Salt Marsh,
849 Wells, ME, USA. *Estuaries Coasts* 32, 855–870. <https://doi.org/10.1007/s12237-009-9203-7>

850 Wilson, K.R., Kelley, J.T., Tanner, B.R., Belknap, D.F., 2010. Probing the origins and stratigraphic
851 signature of salt pools from north-temperate marshes in Maine, U.S.A. *J. Coast. Res.* 1007–1026.
852 <https://doi.org/10.2112/JCOASTRES-D-10-00007.1>

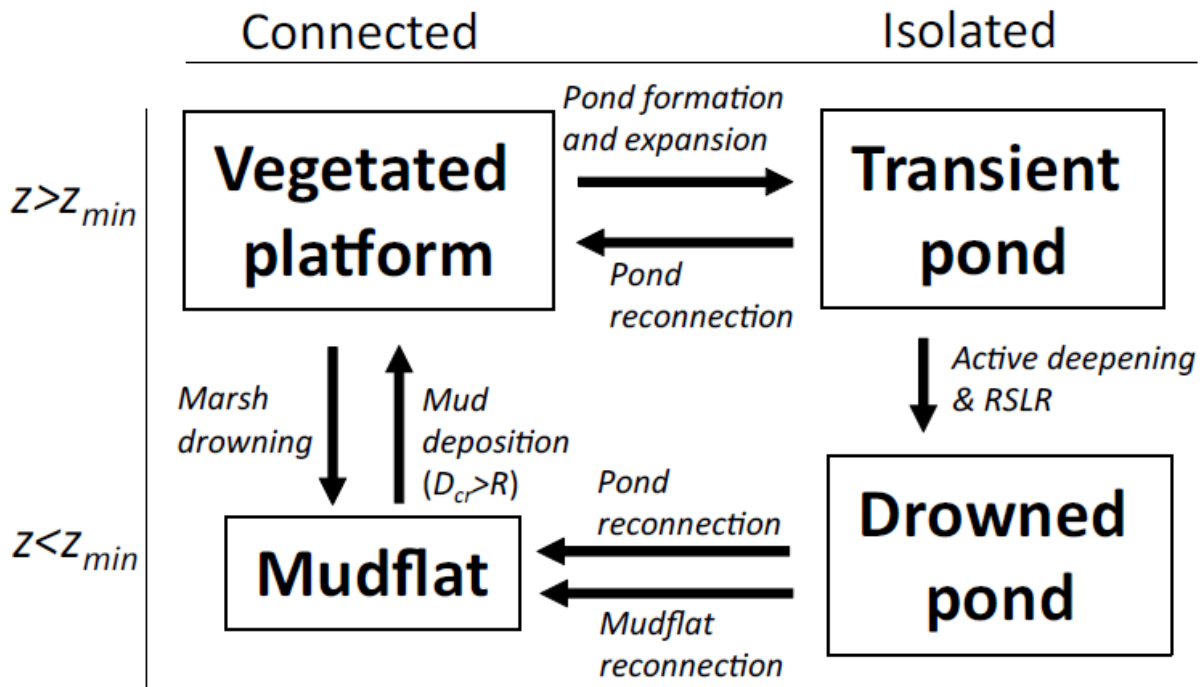
853 Wolfe, R.J., 1996. Effects of open marsh water management on selected tidal marsh resources: a review.
854 *J. Am. Mosq. Control Assoc.* 12, 701–712.
855

856 **List of figures**

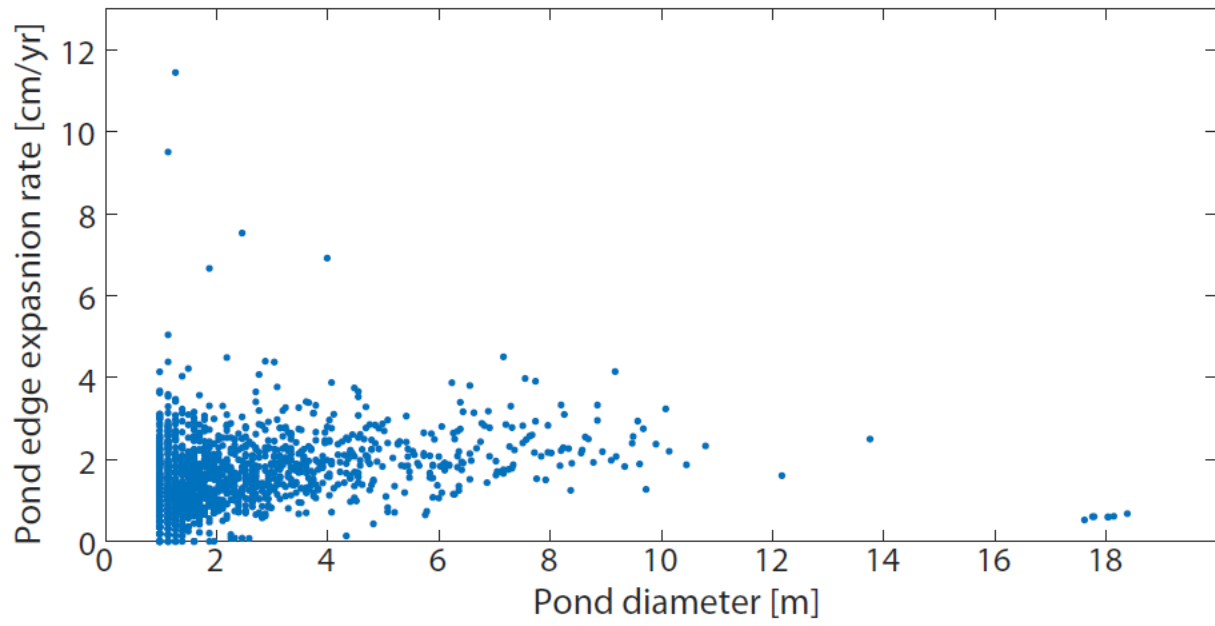


857

858 Figure 1. A) Map of the study area including Barnstable marsh and Sage Lot Pond marsh (Massachusetts,
 859 USA). B) Sage Lot Pond marsh, C) Barnstable marsh. The dashed rectangle outlines the domain used in
 860 the model. The white dots indicate the locations where SSC was measured in triplicates. The red dots
 861 indicated the location where cores for vertical accretion were collected. D,E,F) Example of pond
 862 reconnection and rapid revegetation (the pond is indicated by the arrow on the bottom right of panel C).
 863 G) Location of the surveyed ponds. Red dots indicate ponds surveyed along a transect (showed in Fig. 8),
 864 white dots indicate ponds only surveyed at one edge. H) Detail of a marsh core collected adjacent to the
 865 channel. Images from Google Earth (NASA, USDA) accessed on October 2019.



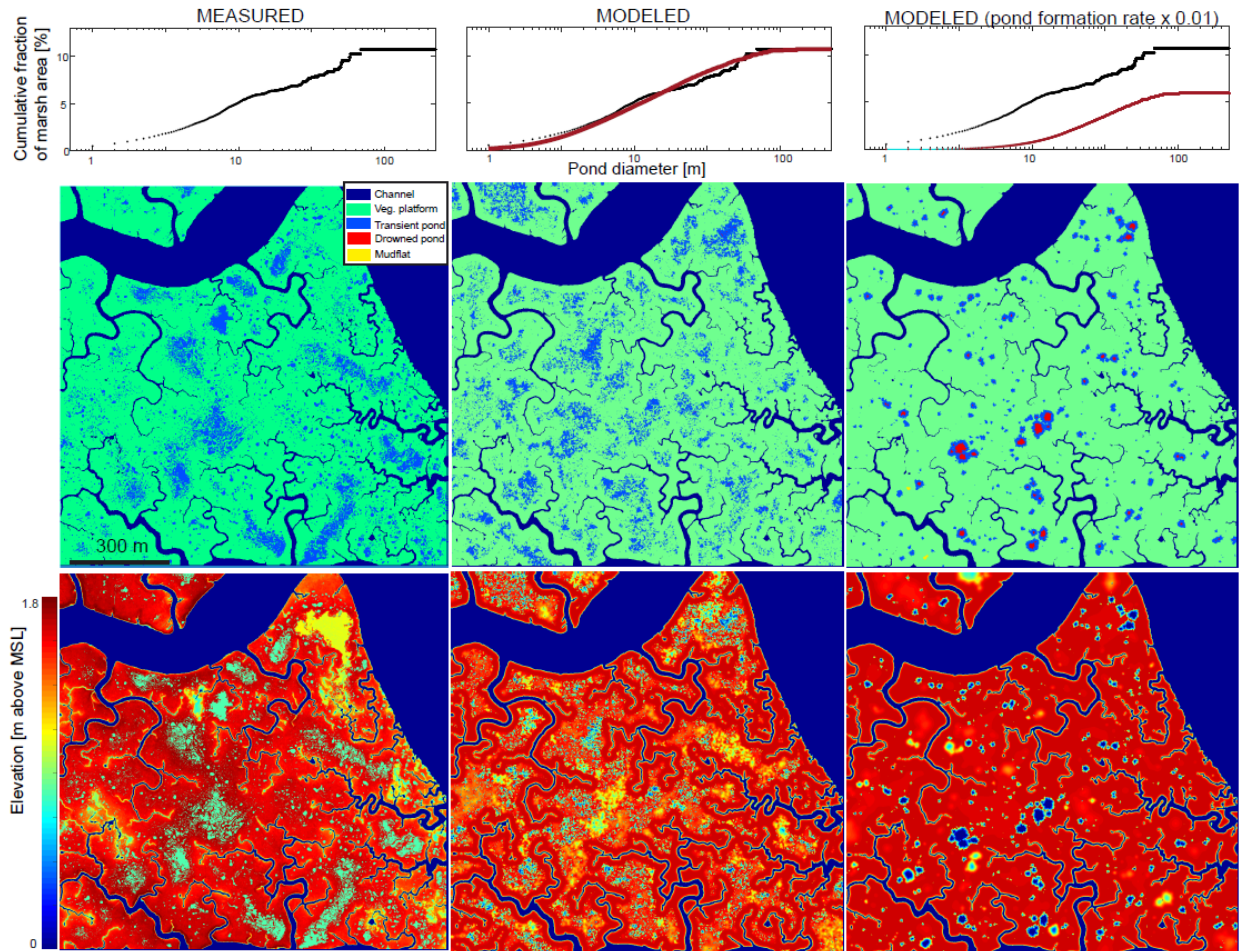
866
 867 Figure 2. Summary schematic of the marsh and pond dynamics and scheme of the various sediment fluxes
 868 in the model. Net vertical accretion is equal to the gross vertical deposition minus bank creep and
 869 ponding.



870

871 Figure 3. Measured pond edge expansion rate as the increase of the pond radius through time in

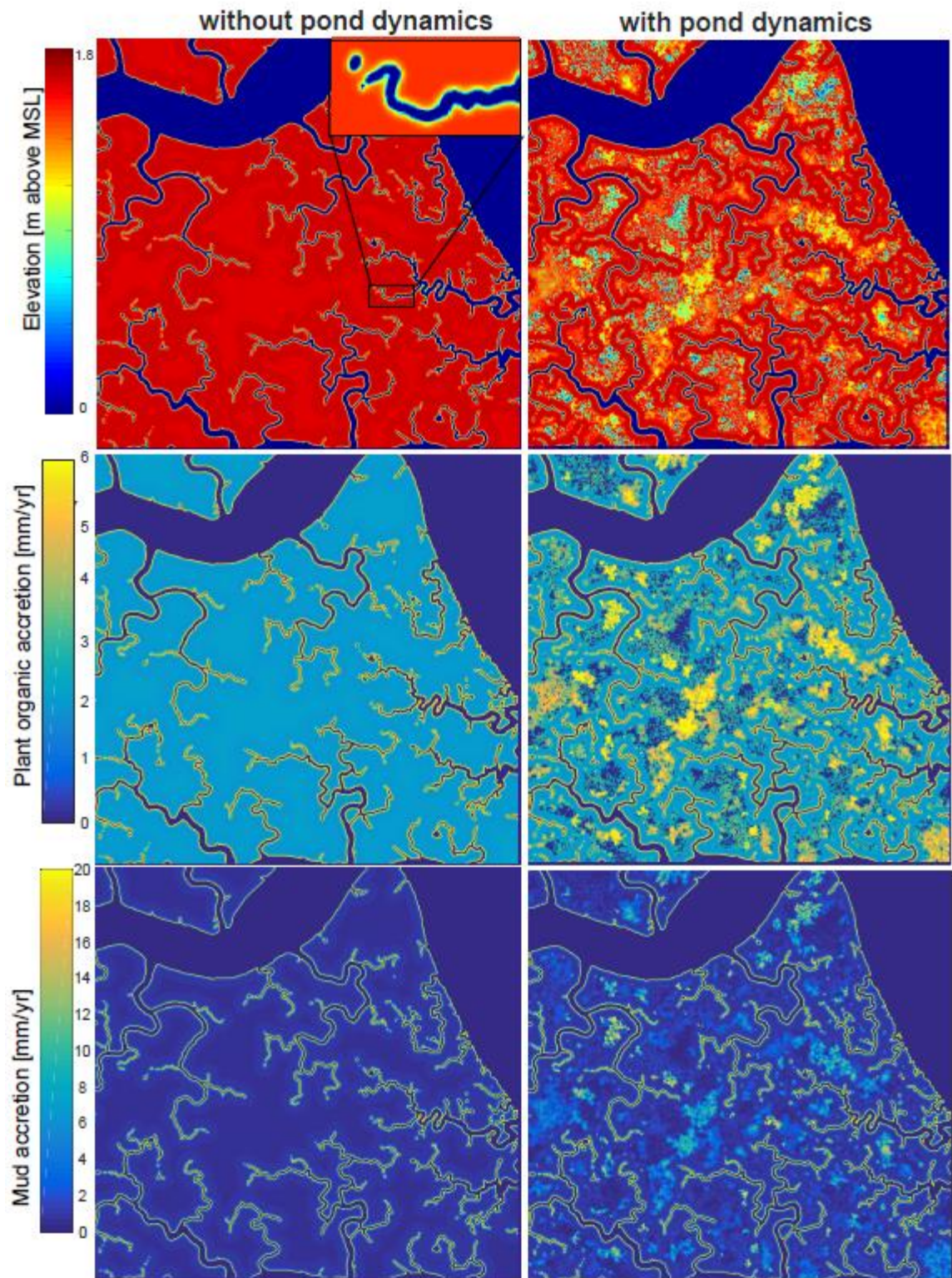
872 Barnstable marsh from 1973 to 2014 as a function of the pond diameter.



873

874 Figure 4. A,B,C) Comparison of measured and simulated (at steady state after 1000 years) pond size
 875 distribution. A) Measured pond size distribution, showing that the total fraction of pond area is about 10%
 876 of the marsh surface. B) Best fit for the parameters k_{seed} and k_{exp} . C) Model results for the case in
 877 k_{seed} is decreased by a factor 100. D,G) Measured pond spatial distribution and elevation E,F,H,I) Model
 878 snapshot after 1000 years showing the pond spatial distribution and the elevation (as the last datapoint in
 879 Fig. 6).

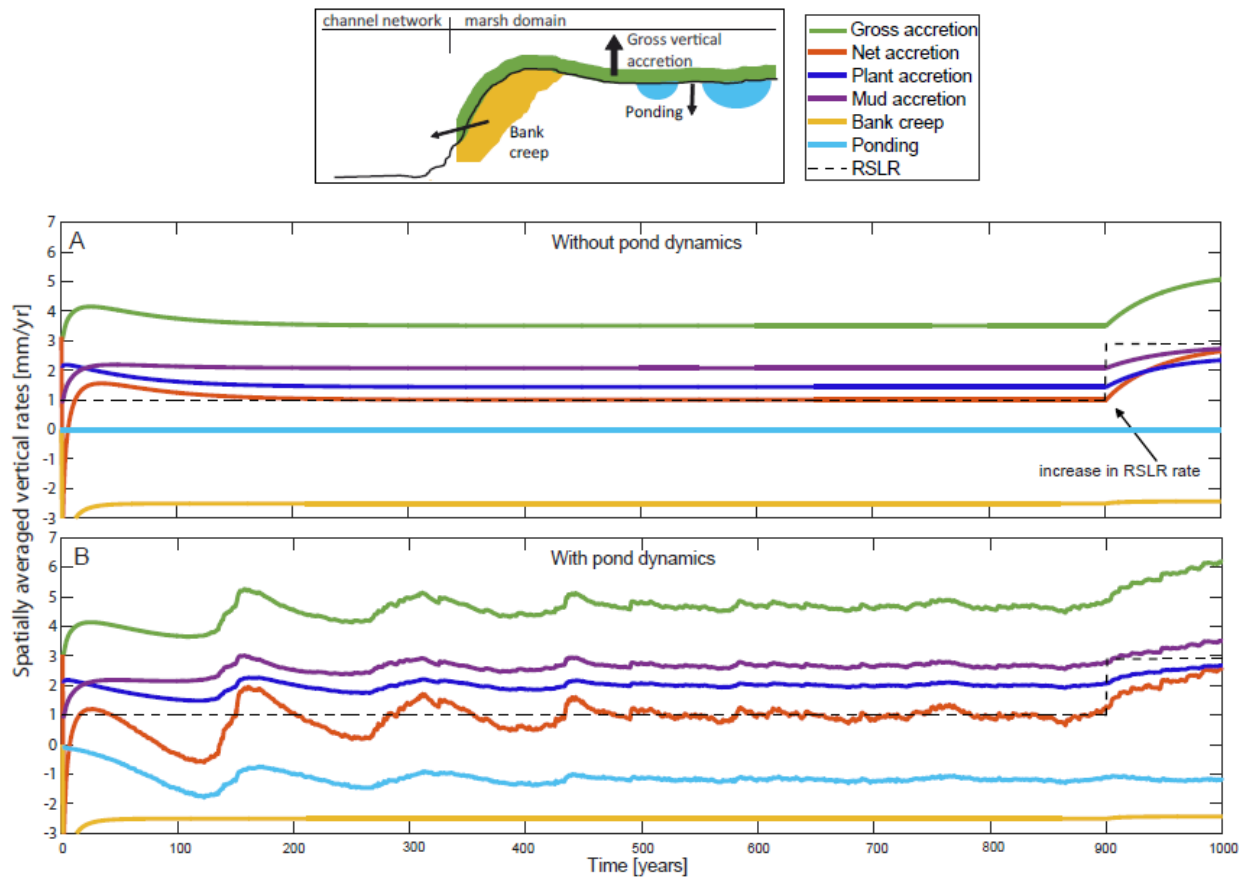
880



881

882 Figure 5. Vertical accretion rate by *in situ* plant production and by mud accumulation for the case with
 883 and without pond dynamics calculated at year 1000 (as the last datapoint in Fig. 6). The inset in the top
 884 left panels shows the detail of the low-marsh adjacent to a channel.

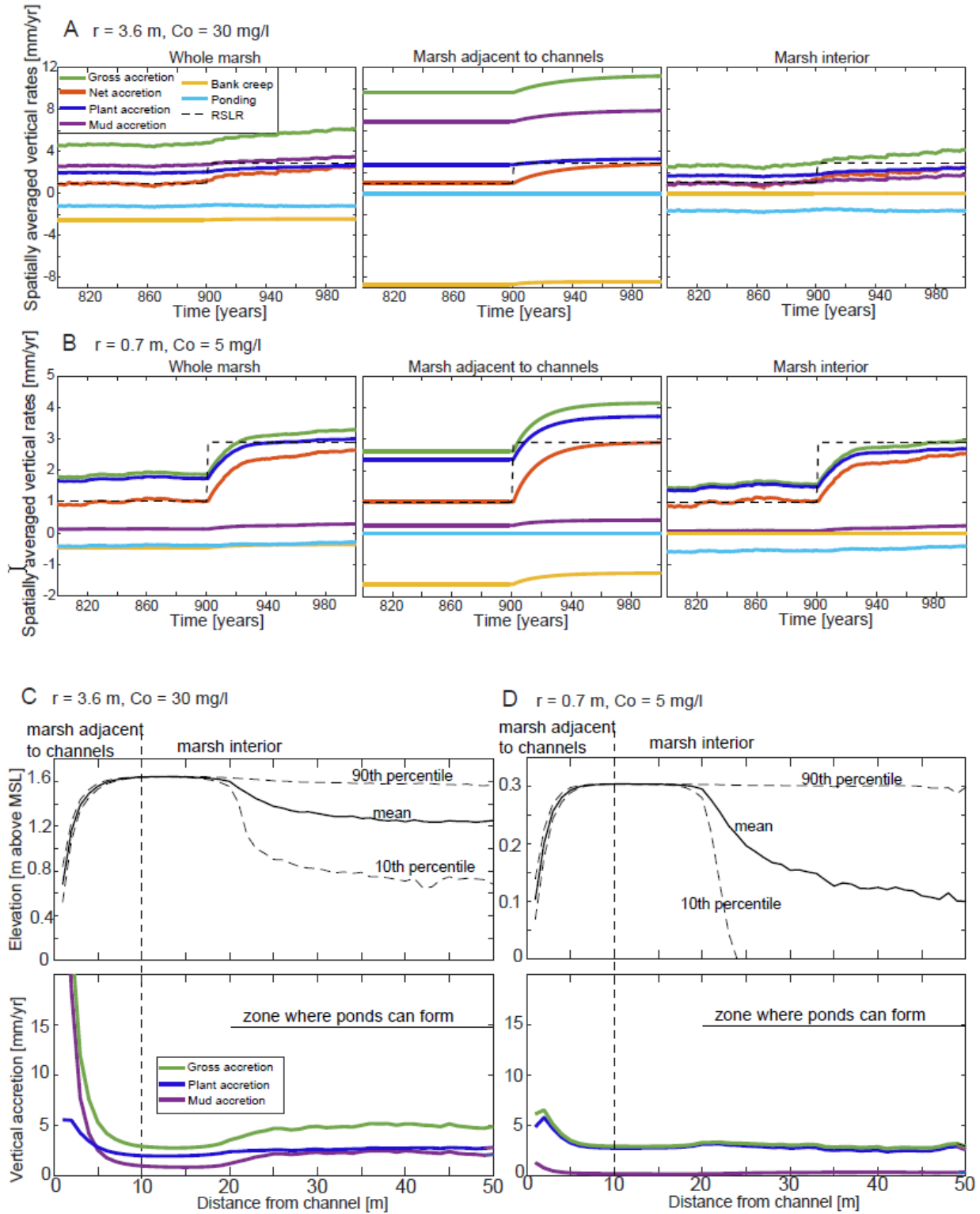
885



886

887 Figure 6. Reconstructed time series of spatially-averaged elevation change for Barnstable marsh,
 888 comparing the case without ponds dynamics (A) and with pond dynamics (B). Gross accretion is the sum
 889 of plant and mud accretion. Net accretion is the gross accretion minus ponding and bank creep. Note that
 890 during the first ~500 years the marsh is equilibrating from the initial conditions without ponds.

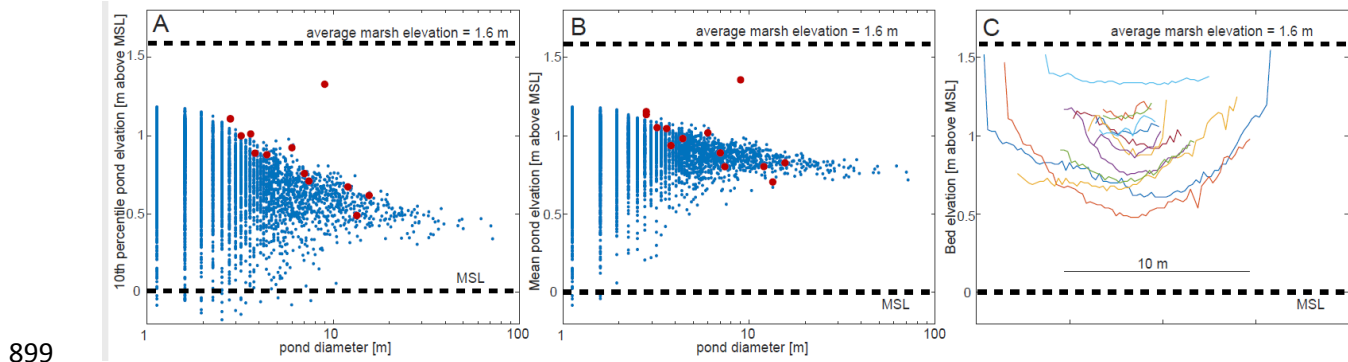
891



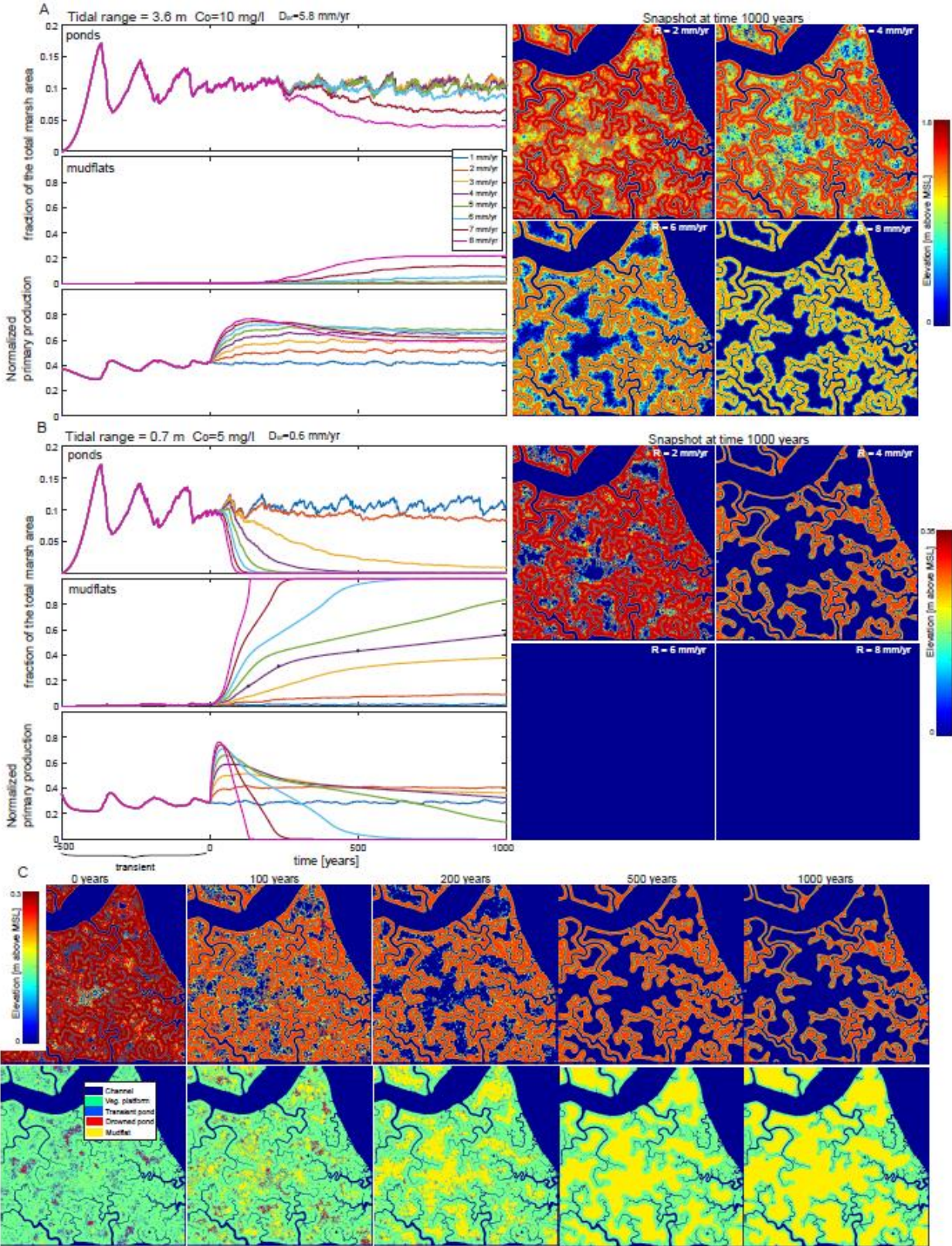
892

893 Figure 7. A,B) Spatially-averaged elevation change during the transition from $R=1$ mm/yr to $R=2.9$
 894 mm/yr (as in Fig. 6B), considering the whole marsh area, the area adjacent to channels, and the marsh

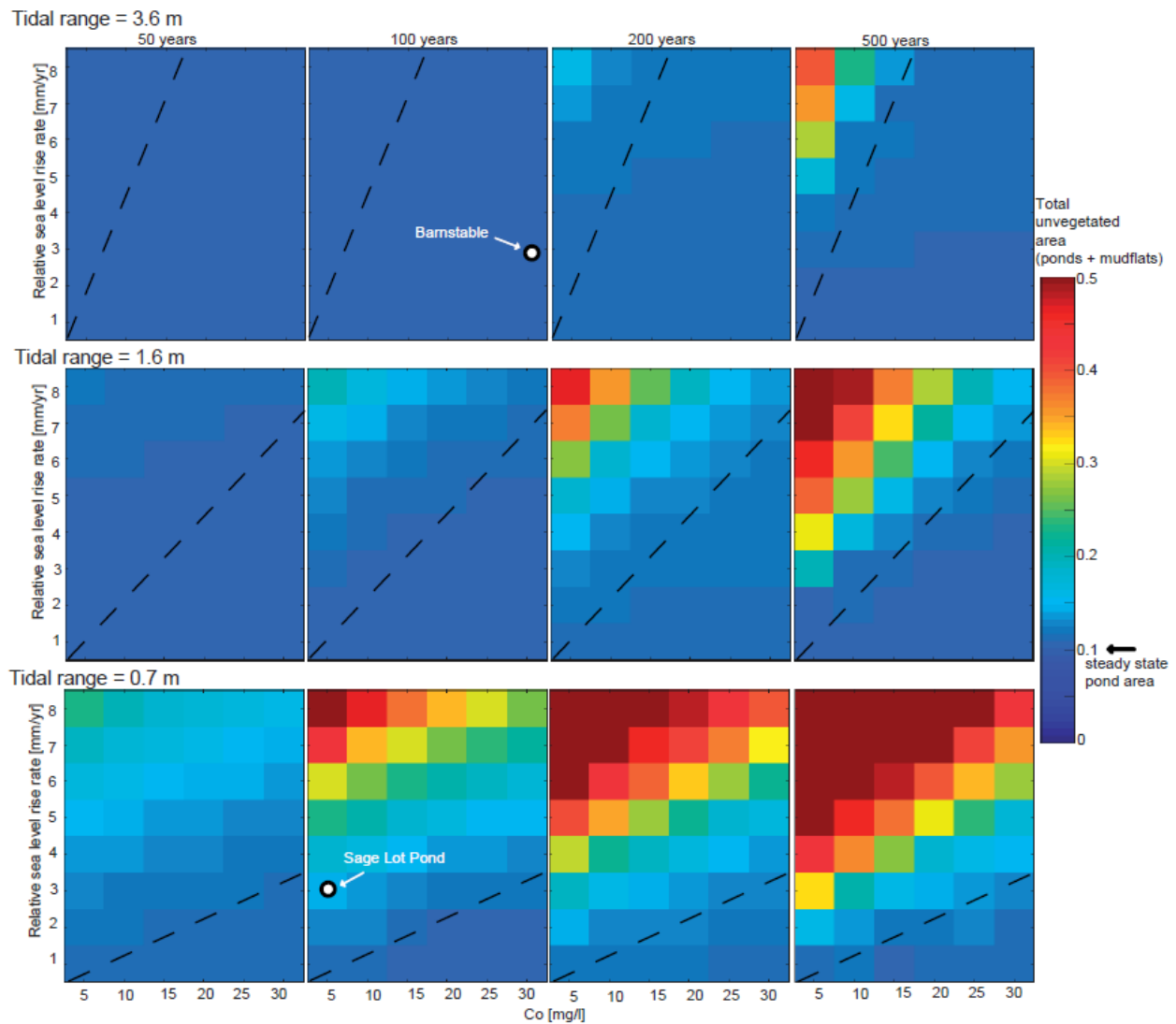
895 interior. Note that in the marsh interior the bank creep is zero. C,D) Snapshot at year 1000 showing the
 896 how the vertical accretion varies rapidly with the distance from the channel network. A,C) Conditions
 897 representing Barnstable marsh ($r=3.6$ m, $C_o=30$ mg/l), B,D) Conditions representing Sage Lot Pond
 898 marsh ($r=0.7$ m, $C_o=5$ mg/l).



900 Figure 8. A,B) Modeled 10th percentile (A) and mean (B) pond elevation as a function of pond size. The
 901 blue dots are the individual points from the model, the red dots are the survey of the 13 ponds in
 902 Barnstable marsh. C) Cross sections of the 13 ponds surveyed in Barnstable marsh (see Fig 1G).



904 Figure 9. A,B) Amount of pond and mudflat area through time for different RSLR rates for the case of
 905 Barnstable marsh ($r=3.6$ m) with a reduced sediment supply ($C_o=10$ mg/l) (A), and for the case of Sage
 906 Lot Pond marsh ($r=0.7$ m and $C_o=5$ mg/l) (B). The normalized primary production is calculated averaging
 907 the plant primary production divided by the maximum primary production (which is attained when the
 908 marsh is at the elevation optimum). The normalized primary production initially increases because the
 909 marsh attains a lower elevation but subsequently decreases when the pond area (whose primary
 910 production is assumed to be zero) increases. C) Snapshots of marsh configurations at different times (as
 911 indicated by the black dots in panel B) for the case of Sage Lot Pond marsh with $R=4$ mm/yr.



912

913 Figure 10. Predictions of total unvegetated area (ponds + mudflats) at different time intervals after the
 914 increase in RSLR rate. The dashed lines indicate the threshold between pond recovery and pond runaway
 915 regime using the lumped pond model of Mariotti (2018), with $R=D_{cr}=\alpha C_o r/(2T\rho_m)$. The comparison with
 916 Barnstable and Sage Lot Pond marsh is made assuming that the increase in relative sea level rise rate
 917 started about 100 years ago at the beginning of the 20th century.

918

919 Table 1. Sediment accretion rates measured on 1 cm sediment core intervals in Barnstable (measured
 920 for this work) and Sage Lot Pond marshes (Gonneea et al., 2019, 2018).

921

Site	Sediment accretion rate (1900 to 2018) mm/y
Sage Lot Pond	
Interior (1 core, 13 intervals)	1.4 ± 0.3
Channel-adjacent (1 core, 27 intervals)	3.6 ± 2.0
Barnstable	
Interior (3 cores, 134 intervals)	5.1 ± 3.3
Channel-adjacent (3 cores, 130 intervals)	4.6 ± 2.5

922

923 Table 2. List of parameters used in the model.

	Symbol	Description	Value	Reference
	Δx	Spatial discretization	1 m	
	Δt	Temporal discretization	1 year	
Physical parameters	C_o	SSC in channels	30 mg/l or 5 mg/l	Measured
	ρ_m	Mud dry bulk density	650 kg/m ³	Assumed
	β	Horizontal decay rate of SSC with distance from channel network	0.05 m ⁻¹	(Christiansen et al., 2000)
	α	Fraction of spatially uniform SSC	0.3	Assumed

	r	Spring tidal range	3.6 m or 0.7 m	NOAA Station 8447930 and Station 8447241
	Δr	Spring-neap variability	$0.05r$	NOAA
	T	Tidal period	12.5 hr	NOAA
	R	Relative Sea Level Rise rate	2.9 mm/yr	NOAA
	μ	Soil creep diffusivity	$0.1 \text{ m}^2/\text{yr}$	(Mariotti et al., 2019)
Vegetation parameters	z_{min}	Min elevation for vegetation	0	Assumed
	z_{max}	Max elevation for vegetation	$r/2$	Assumed
	D_{pMAX}	Max in-situ organic deposition	6 mm/yr	Assumed
Pond Parameters	k_{seed}	Pond formation rate	$4 \cdot 10^{-4}$ #ponds/m ² /yr	Calibrated
	k_{exp}	Pond expansion rate	0.015 m/yr	Measured
	L	Drainage influence length	20 m	Measured
	Y_{pond}	Max initial depth of new ponds	$0.25(z_{max} - z_{min})$	Calibrated
	$P_{deepening}$	Active deepening of ponds	3 mm/yr	Calibrated

924

925